Anharmonic theoretical simulations of infrared spectra of halogenated organic compounds

Cite as: J. Chem. Phys. **139**, 074310 (2013); https://doi.org/10.1063/1.4817401
Submitted: 02 May 2013 . Accepted: 18 July 2013 . Published Online: 21 August 2013

Ivan Carnimeo, Cristina Puzzarini, Nicola Tasinato, Paolo Stoppa, Andrea Pietropolli Charmet, Malgorzata Biczysko, Chiara Cappelli, and Vincenzo Barone

Anharmonic theoretical simulations of infrared spectra of halogenated organic compounds

Ivan Carnimeo,[1,2,3,a)] Cristina Puzzarini,[4] Nicola Tasinato,[5] Paolo Stoppa,[5] Andrea Pietropolli Charmet,[5] Malgorzata Biczysko,[2,6] Chiara Cappelli,[1,2] and Vincenzo Barone[2,3]

[1]*Dipartimento di Chimica e Chimica Industriale, Università di Pisa, Via Risorgimento 35, I-56126 Pisa, Italy*
[2]*Scuola Normale Superiore, Piazza dei Cavalieri 7, I-56126 Pisa, Italy*
[3]*Istituto Nazionale di Fisica Nucleare, Sezione di Pisa, Polo Fibonacci Largo B. Pontecorvo 3, I-56127 Pisa, Italy*
[4]*Dipartimento di Chimica "Giacomo Ciamician", Università degli Studi di Bologna, Via Selmi 2, I-40126 Bologna, Italy*
[5]*Dipartimento di Scienze Molecolari e Nanosistemi, Università Cà Foscari Venezia, Calle Larga S. Marta 2137, I-30123 Venezia, Italy*
[6]*Istituto Italiano di Tecnologia, Center for Nanotechnology Innovation, NEST, I-56127 Pisa, Italy*

(Received 2 May 2013; accepted 18 July 2013; published online 21 August 2013)

The recent implementation of the computation of infrared (IR) intensities beyond the double-harmonic approximation [J. Bloino and V. Barone, J. Chem. Phys. **136**, 124108 (2012)] paved the route to routine calculations of infrared spectra for a wide set of molecular systems. Halogenated organic compounds represent an interesting class of molecules, from both an atmospheric and computational point of view, due to the peculiar chemical features related to the halogen atoms. In this work, we simulate the IR spectra of eight halogenated molecules (CH_2F_2, $CHBrF_2$, CH_2DBr, CF_3Br, CH_2CHF, CF_2CFCl, cis-CHFCHBr, cis-CHFCHI), using two common hybrid and double-hybrid density functionals in conjunction with both double- and triple-ζ quality basis sets (SNSD and cc-pVTZ) as well as employing the coupled-cluster theory with basis sets of at least triple-ζ quality. Finally, we compare our results with available experimental spectra, with the aim of checking the accuracy and the performances of the computational approaches. © *2013 AIP Publishing LLC*. [http://dx.doi.org/10.1063/1.4817401]

I. INTRODUCTION

The growing concerns of scientific communities and international politicians about global climate changes and environmental degradation related to human activities have pointed out the need for a deeper knowledge of atmospheric chemical and physical processes in order to understand and predict the evolution of the Earth's atmosphere. Over the past years, halogenated organic compounds – in particular those containing chlorine and bromine – were widely used in anthropogenic activities due to their desirable properties as blowing agents, propellants, refrigerants, fire extinguishers, and as reactants in the industrial synthesis of polymers and copolymers. However, with few exceptions, since 1996 these compounds have been phased out by the Montreal protocol (and the Copenhagen amendment), given their capacity to destroy the stratospheric ozone layer and to behave as greenhouse gases.[1–3] In fact, they can exercise an additional radiative forcing that tends to warm the climate, contributing to global warming. Several research efforts have been devoted to the study of the radiative forcing and, in general, the spectroscopic behavior of the halogenated organics, with aim of assessing the environmental impacts of these compounds, considering the brief- and long-term environmental effects, as well as the contribution to climate changes and global warming (see, for example, Refs. 4–7). Indeed, the macroscopic radiation and atmospheric models, employed to understand the atmospheric chemistry as well as to model the Earth's atmosphere and its evolution, need as an input a detailed dataset.[8–10] Within this framework, infrared (IR) spectroscopy plays a primary role,[11–21] as it can provide accurate values of the relevant spectroscopic data, such as band positions and absorption cross sections. With these premises, it is not surprising that the last years have seen a renewed interest in the spectroscopic studies of halogenated organic compounds, motivated not only by their role as air pollutants, but also because these investigations are useful to improve the modeling of the atmospheric chemistry of these compounds.[22–25]

In this context, the prediction of molecular properties by state-of-the-art quantum-mechanical (QM) methods has been proved of paramount relevance for the study of molecular systems. In the last years, theoretical computations have become powerful and widespread tools for the assignment and prediction of the experimental spectra, as well as to get deeper insight into the different effects that determine the observed spectroscopic properties.[26–29,91] As far as IR spectroscopy is concerned, QM calculations carried out at a suitable level of theory allow the prediction of reliable vibrational spectra for small- to medium-sized molecules (for example, see Refs. 21, 30–36 and references therein) In this

a)Electronic mail: ivan.carnimeo@sns.it

respect, while approaches based on vibrational perturbation theory (VPT2)[33,34,37–42] have been shown capable of accurately calculating vibrational frequencies, comparatively less attention has been paid to infrared intensities beyond the double-harmonic approximation. With the recent implementation of the calculation of intensities at a fully anharmonic VPT2 level,[43,44] the simulation of the whole infrared spectrum becomes feasible, and a theoretical study of both peak positions and absorption intensities of halons can be performed. Thus, new insights to the characterization of molecules taking part in chemical processes of atmospheric interest can be achieved. From a computational and methodological point of view, the presence of halogen atoms is particularly challenging, since such elements show large electronegativities and, the heaviest ones, significant relativistic core-electron effects. For this reason, most of the studies performed in past years[16–18,20,21,45–47] were carried out at the coupled-cluster (CC) level[48] employing medium-to-large basis sets (at least of triple-ζ quality). Unfortunately, the very high accuracy which usually characterizes such calculations implies a large computational cost, and can be performed only for small- to medium-sized systems. The situation turns out to be more involved with the halogen atoms, because they are characterized by a large number of valence electrons, and the calculations at the coupled-cluster level might become particularly expensive when a few of them are present in the molecules under study. This is especially true when the heaviest atoms are involved, for which the explicit treatment of the *d*-electrons is required in most of cases.

Density Functional Theory (DFT) based approaches are the methods of choice to treat medium- to large-sized systems. Provided that both the functional and the basis set are carefully chosen, DFT has been demonstrated to provide accurate vibrational anharmonic frequencies, for both small- and medium-sized molecular systems,[32,42,44,49,50] in conjunction with a full-dimensional VPT2 approach, and for large systems, using purposely tailored reduced-dimensionality versions of the VPT2 treatment.[51,52] DFT methods can also be used in hybrid approaches, in which the harmonic and anharmonic parts of the frequencies and intensities are calculated at different levels of theory. Such approaches – coupling coupled-cluster and DFT[53–59] or even two DFT methods employing different combinations of functional and basis set[44] – have been applied to several cases,[44,53–60] leading to a remarkable agreement with experimental data, at a reduced computational cost with respect to the full coupled-cluster treatment.

In the present work, we selected a set of eight small halogenated hydrocarbons, four methane derivatives (halomethanes: CH_2F_2, $CHBrF_2$, CH_2DBr, CF_3Br) and four ethylene derivatives (halo-ethylenes: CH_2CHF, CF_2CFCl, cis-CHFCHI, cis-CHFCHBr), and we simulated the infrared spectra at a full anharmonic level employing different DFT methods (see Sec. II C for details). Hybrid approaches have also been considered for both frequency and intensity calculations. The results of the different approaches were compared with the available experimental data in order to verify the reliability of the DFT methods, discuss strengths and weaknesses of each model, and provide statistics about the accuracy that could be expected. In our opinion, such a work paves the route to the routine application of DFT methods to the calculation of spectroscopic properties of medium-to-large halogenated systems.

II. METHODOLOGY AND COMPUTATIONAL DETAILS

A. Theoretical modeling of infrared spectra

When a vibrational spectrum is experimentally measured, the absolute intensity and width of the vibrational features are determined by the physico-chemical processes due to light-matter interaction as well as by parameters and/or conditions intrinsically connected to the typology of the experiment, such as the optical pathlength of the instrument and the concentration/partial pressure of the sample. For this reason, the measured *absorbance* is usually converted into the *absorption cross section* (cm^2/molecule), which is an intrinsic molecular property, independent of the experimental conditions. Nonetheless, the band intensity given in terms of *absorption cross section* is still the result of the evolution of the system after the irradiation, since the processes occurring during the relaxation dynamics usually affect the spectral features. Moreover, in most cases the experimental spectra show many complex low-intensity features, related to overtones and combination bands, resonances, or to the rotational structure of the vibrational transitions. Consequently, the experimental intensities are usually integrated over a selected range of frequencies, say $[\nu_1, \nu_2]$, in order to obtain the *integrated absorption cross section*[17,18,61] ($G_{\nu_1\nu_2}$). $G_{\nu_1\nu_2}$ is the area subtended by a region of the spectrum, and it can be calculated by *ab initio* methods with time-independent approaches. A formal expression for the *absorption cross section* can be obtained from the treatment of the light-matter interaction, and the molar counterpart (i.e., the *molar absorption coefficient*) can be written as[62]

$$\varepsilon(\nu) = \frac{4N_A\pi^2}{3 \times 10^3 \ln(10)hc}\nu \sum_{i,f} \rho_i |\mu_{if}|^2 \delta(\nu_{if} - \nu). \quad (1)$$

In Eq. (1), i and f are two generic initial and final purely vibrational states, $\nu_{if} = \nu_i - \nu_f$ being the corresponding frequency difference; ρ_i is the Boltzmann population of the state i, μ_{if} is the transition moment, and N_A is the Avogadro constant (mol^{-1}). The spectral line shape is given here by the Dirac delta function since no information about the relaxation dynamics can be obtained at this level of theory.

By integrating the *molar absorption coefficient* in a frequency interval $[\nu_1, \nu_2]$, we obtain the theoretical *integrated cross section* (usually in km/mol)

$$G_{\nu_1,\nu_2} = \int_{\nu_1}^{\nu_2} \varepsilon(\nu) d\nu = \frac{4N_A\pi^2}{3 \times 10^3 \ln(10)hc} \sum_{\substack{i,f \\ \nu_1 < \nu_{if} < \nu_2}} \rho_i |\mu_{if}|^2 \nu_{if} = \sum_{\substack{i,f \\ \nu_1 < \nu_{if} < \nu_2}} G_{if}, \quad (2)$$

which is the sum of the *integrated cross section* of each transition (G_{if}) occurring in the selected frequency range. The G_{if} quantities can be obtained within either the harmonic

or anharmonic approximations. In this work, the latter approach, as implemented by Barone *et al.*[43,63] into the Gaussian code,[64] has been applied to compute the G_{if} related to fundamental transitions, overtones, and combination bands. Once the G_{if}'s are known, G_{ν_1,ν_2} (Eq. (2)) can be straightforwardly calculated, whereas the *absorption cross sections* in cm^2/molecule can be obtained by a convolution with Gaussian (or Lorentzian) functions $g_{FWHM}(\nu)$, thus allowing a direct comparison between simulated and experimental IR spectra. Since no information about the relaxation dynamics can be obtained at this level of theory, the FWHM (Full Width at Half Maximum) of either the Gaussian or Lorentzian function considered is simply an adjustable, empirical parameter

$$\varepsilon_g(\nu) = \varepsilon(\nu') * g_{FWHM}(\nu - \nu') = \sum_{i,f} G_{if} g_{FWHM}(\nu_{if} - \nu). \tag{3}$$

B. Coupled cluster methods

The CC level of theory employing the CC singles and doubles approximation augmented by a perturbative treatment of the triple excitations [CCSD(T)][65] has been used in the reference computations described below, in conjunction with correlation-consistent basis sets, (aug-)cc-p(C)VnZ (n = T,Q).[66–68] At the geometries optimized at the levels of theory considered, the corresponding harmonic force fields (at the same level) have been obtained using analytic second derivatives.[69] All CCSD(T) calculations have been carried out with the quantum-chemical CFOUR program package.[70]

For each molecule, we chose a reference set of CCSD(T) results in order to validate the geometries, harmonic frequencies, and IR intensities at the DFT level. For the CH_2F_2 and CH_2CHF molecules, we were able to compute the full Hessian at the CCSD(T)/aug-cc-pVQZ level and to also include core-valence (CV) correlation corrections at the CCSD(T)/cc-pCVTZ level (shortly, denoted as "CCSD(T)/AVQZ+CV"). For details concerning the additivity scheme, we refer interested readers to Refs. 35, 58–60, 71, and 72. The "CCSD(T)/AVQZ+CV" approach is expected to yield values on average accurate within 2 cm^{-1}, that is to say, due to a cancelation of errors, to have the same accuracy of harmonic frequencies obtained by means of the extrapolation to complete basis set (CBS) in conjunction with the inclusion of core correlation, scalar relativistic, and higher order correlation effects.[36,73,74] When heavy atoms – chlorine, bromine, and iodine – were involved, we used triple-ζ quality basis sets for CCSD(T) calculations, i.e., aug-cc-pVTZ for methane-derivatives ($CHBrF_2$, CH_2DBr, CF_3Br) and cc-pVTZ for ethylene-derivatives (CF_2CFCl, cis-CHFCHBr, cis-CHFCHI). In Sec. III, a detailed discussion about the reasons leading to the choice of such basis sets is reported. For bromine and iodine, the cc-pVTZ-PP and aug-cc-pVTZ-PP sets[75,76] were actually used in order to take into account relativistic effects. The latter are correlation-consistent basis sets to be used in conjunction with small-core relativistic pseudopotentials that leave 25 electrons to be handled explicitly for both Br and I. In the following, the different basis sets used for the reference coupled-cluster calculations will be generically indicated as REF, and in Table I a summary of the CCSD(T)/REF level for each molecule is reported.

TABLE I. Summary of the reference methods.

Molecule	CCSD(T)/REF
CH_2F_2	aug-cc-pVQZ+CV
$CHBrF_2$	aug-cc-pVTZ-PP
CH_2DBr	aug-cc-pVTZ-PP
CF_3Br	aug-cc-pVTZ-PP
CH_2CHF	aug-cc-pVQZ+CV
CF_2CFCl	cc-pVTZ
cis-CHFCHBr	cc-pVTZ-PP
cis-CHFCHI	cc-pVTZ-PP

C. DFT methods

The DFT calculations have been performed with the B3LYP[77] functional in conjunction with the double-ζ SNSD[78] basis set family, which is an improved version of the polarized double-ζ N07D basis set,[58,78–81] obtained by adding diffuse *s*-functions on all atoms, diffuse polarized *d*-functions on heavy atoms (*p* on hydrogens), and Stuttgart-Dresden electron core pseudopotentials[82,83] to bromine and iodine. In fact, although the original N07D provided very good results in the computation of frequencies and EPR properties,[29,35,44,52,58–60,71,72,78–81] the inclusion of diffuse functions and pseudopotentials are needed to properly treat the heaviest halogen atoms and to improve the performances of the IR intensity calculations. The double-hybrid B2PLYP[84,85] functional, along with its analytic second derivatives[50] required for the effective computation of semi-diagonal quartic force-fields, was also employed in conjunction with the cc-pVTZ basis set (cc-pVTZ-PP in case of Br and I). Despite the fact that the inclusion of a portion of the MP2[86] energy and the use of a triple-ζ basis set lead to a significantly higher computational cost, such a method usually provides very accurate harmonic frequencies[50] and may improve anharmonic corrections in problematic cases.[72] As an intermediate computational approach between the B3LYP/SNSD and B2PLYP/cc-pVTZ(-PP) levels, we also performed calculations at the B3LYP/cc-pVTZ(-PP) level for one halo-methane ($CHBrF_2$) and one halo-ethylene (CF_2CFCl) in order to evaluate the effects of the functional and the basis set on the accuracy of the vibrational properties. All DFT geometry optimizations (tight convergence criteria) and harmonic-frequency calculations have been performed by constraining the molecules to the proper symmetry point groups, so that the symmetry of each normal mode could be verified. Subsequently, the cubic and semi-diagonal quartic force constants have been obtained by numerical differentiation of the analytical second derivatives (with a step of 0.01 Å as discussed in Ref. 34), starting from the equilibrium structure without any symmetry constraint. Then, the IR spectra have been simulated from the anharmonic force field by means of a fully automated VPT2 approach, originally developed for the calculation of the anharmonic

TABLE II. CH_2F_2: Convergence of the CCSD(T) harmonic frequencies (cm^{-1}) with respect to the dimension of the basis set.[a]

Modes	Symm.	CCSD(T)/ cc-pVTZ	CCSD(T)/ aug-cc-pVTZ	CCSD(T)/ cc-pVQZ	CCSD(T)/ aug-cc-pVQZ	CCSD(T)/ AVQZ+CV	Assignments[b]
ν_6	B_1	3148.0 (−11.8)	3150.5 (−9.3)	3155.0 (−4.7)	3155.0 (−4.8)	3159.8	CH_2 A stretch
ν_1	A_1	3075.8 (−8.9)	3076.6 (−8.1)	3081.5 (−3.2)	3079.7 (−5.0)	3084.7	CH_2 S stretch
ν_2	A_1	1556.5 (4.5)	1552.8 (0.8)	1553.7 (1.6)	1549.8 (−2.2)	1552.0	CH_2 scissor
ν_8	B_2	1482.3 (12.5)	1466.2 (−3.6)	1475.6 (5.7)	1467.4 (−2.4)	1469.8	CH_2 wag
ν_5	A_2	1292.3 (4.2)	1279.4 (−8.7)	1290.1 (2.0)	1285.0 (−3.1)	1288.1	CH_2 twist
ν_7	B_1	1202.6 (3.5)	1192.2 (−6.9)	1201.7 (2.6)	1197.1 (−2.0)	1199.1	CH_2 rock
ν_3	A_1	1141.6 (7.7)	1126.6 (−7.3)	1136.9 (3.0)	1131.4 (−2.5)	1133.9	CF_2 S stretch
ν_9	B_2	1142.2 (22.9)	1113.6 (−5.7)	1127.1 (7.7)	1117.0 (−2.3)	1119.3	CF_2 A stretch
ν_4	A_1	537.0 (2.3)	529.7 (−5.0)	536.0 (1.2)	533.1 (−1.6)	534.7	CF_2 bend
MAE[c]		8.7	6.2	3.6	2.9	0.0	

[a]Differences with respect to the CCSD(T)/AVQZ+CV level are reported in parenthesis.
[b]A and S refer to Asymmetric and Symmetric modes, respectively.
[c]The Mean Absolute Error (MAE) for each basis set has been calculated by averaging the absolute errors on each mode.

frequencies[33,34,42] and recently extended to intensities[43] of fundamentals, overtones, and combination bands. Within this approach, resonant terms are removed from the perturbative expansion and variationally treated, i.e., the so-called GVPT2 approach[34] has been applied for frequency calculations. A deperturbed approach was used instead for the resonant terms of the perturbative treatment of the dipole moment derivatives. All calculations have been performed with a locally modified version of Gaussian code.[64]

D. Hybrid approach

Hybrid CC/DFT models (shortly denoted HYB) assume that the differences between anharmonic frequencies and IR intensities calculated at the CCSD(T) and DFT levels are only due to the harmonic terms. Consequently, the hybrid anharmonic frequency of each normal mode (ν_i^{HYB}) can be viewed as the sum of a harmonic part ($\nu_i^{0,\mathrm{CC}}$) and an anharmonic shift ($\Delta\nu_i^{\mathrm{DFT}}$), computed at the CCSD(T) and DFT levels, respectively

$$\nu_i^{\mathrm{HYB}} = \nu_i^{0,\mathrm{CC}} + \Delta\nu_i^{\mathrm{DFT}}. \tag{4}$$

The anharmonic shifts are evaluated by computing the cubic and semi-diagonal quartic force constants at the DFT level and, as long as the DFT normal modes are similar to the CCSD(T) ones (as expected in most of cases), including them into the VPT2 treatment without any transformation, along with the CCSD(T) harmonic frequencies. Then, in order to grant consistent results independently of the level of theory used to evaluate the cubic and quartic force constants, the Fermi resonances are identified by analyzing the CC harmonic frequencies, the resonant terms being subsequently treated within the variational GVPT2 approach. In this work for the harmonic frequencies, which include the largest part of the errors, we carried out calculations at the CCSD(T)/REF level, while the two DFT methods presented in Sec. II C were used for the computation of the anharmonic shifts. While for frequencies the partitioning between harmonic part and anharmonic shift can be formally justified, for IR intensities (G_{if} in Eq. (1)) an analogous approach can be employed only as an empirical *a posteriori* correction

$$G_{if}^{\mathrm{HYB}} \sim G_{if}^{0,\mathrm{CC}} + \Delta G_{if}^{\mathrm{DFT}}. \tag{5}$$

In fact, from a formal point of view the total transition moment (μ_{if}) can be rigorously split between the sum of the double harmonic transition moment (μ_{if}^0) and an anharmonic shift ($\Delta\mu_{if}$) which includes both mechanical and electric anharmonicities, but since it is squared, in Eq. (1) the cross terms could not be neglected when the *integrated cross section* are computed

$$\begin{aligned} \left|\mu_{if}^0 + \Delta\mu_{if}\right|^2 &= \left|\mu_{if}^0\right|^2 + 2\left|\mu_{if}^0 \cdot \Delta\mu_{if}\right|^2 + \left|\Delta\mu_{if}\right|^2 \\ &\neq \left|\mu_{if}^0\right|^2 + \left|\Delta\mu_{if}\right|^2 . \end{aligned} \tag{6}$$

Nonetheless, the results from this work and earlier studies[35,44,60,71,72] point out the reliability of such an empirical approach, which is thus useful in order to improve the accuracy of computed intensities.

In the following, we will use the notation DFT/DFT, HYB/DFT, HYB/HYB for the IR spectra, indicating that both frequencies and intensities are calculated at the DFT level (DFT/DFT), hybrid frequencies are combined with the DFT intensities (HYB/DFT), and the hybrid approach has been applied to both frequencies and intensities (HYB/HYB), respectively.

III. RESULTS AND DISCUSSION

A. Convergence of CCSD(T) calculations

To establish the reference level of theory to be applied in the subsequent analysis, the convergence of the CCSD(T) results has been inspected by analyzing the data obtained for difluoromethane and 1-fluoroethylene. In Tables II and III, the harmonic frequencies of CH_2F_2 and CH_2CHF, respectively, have been reported. The harmonic frequencies for both molecules have been computed at the CCSD(T) level, in conjunction with the cc-pVTZ (VTZ), aug-cc-pVTZ (AVTZ), cc-pVQZ (VQZ), and aug-cc-pVQZ (AVQZ) basis sets, as well as by means of the composite scheme CCSD(T)/aug-cc-pVQZ+CV(CCSD(T)/cc-pCVTZ) (CCSD(T)/AVQZ+CV). For each normal mode, the frequency differences with respect

TABLE III. CH_2CHF: Convergence of the CCSD(T) harmonic frequencies (cm^{-1}) with respect to the dimension of the basis set.[a]

Modes	Symm.	CCSD(T)/ cc-pVTZ	CCSD(T)/ aug-cc-pVTZ	CCSD(T)/ cc-pVQZ	CCSD(T)/ aug-cc-pVQZ	CCSD(T)/ AVQZ+CV	Assignments[b]
ν_1	A′	3274.0 (−10.9)	3273.5 (−11.4)	3282.1 (−2.8)	3279.5 (−5.4)	3284.9	CH_2 A stretch
ν_2	A′	3214.5 (−10.4)	3215.4 (−9.5)	3220.7 (−4.2)	3219.8 (−5.1)	3224.9	CH stretch
ν_3	A′	3172.2 (−8.4)	3171.7 (−8.9)	3178.4 (−2.2)	3175.3 (−5.3)	3180.6	CH_2 S stretch
ν_4	A′	1698.9 (−2.3)	1691.1 (−10.1)	1700.2 (−1.0)	1696.4 (−4.8)	1701.2	C=C stretch
ν_5	A′	1421.2 (5.2)	1410.8 (−5.2)	1416.5 (0.5)	1413.5 (−2.5)	1416.0	CH_2 bend
ν_6	A′	1332.8 (−1.2)	1326.8 (−7.2)	1332.7 (−1.3)	1331.3 (−2.7)	1334.0	CHF bend
ν_7	A′	1177.7 (−1.7)	1172.3 (−7.1)	1180.7 (1.3)	1176.6 (−2.8)	1179.4	CF stretch
ν_{10}	A″	956.4 (1.7)	942.4 (−12.3)	953.1 (−1.6)	952.0 (−2.7)	954.7	(oop) torsion
ν_8	A′	940.4 (−1.5)	935.7 (−6.2)	941.3 (−0.6)	939.8 (−2.1)	941.9	CH_2 rock
ν_{11}	A′	874.6 (−4.6)	865.5 (−13.7)	873.1 (−6.1)	874.6 (−4.6)	879.2	(oop) CH_2 S bend
ν_{12}	A″	729.3 (1.3)	719.4 (−8.6)	726.7 (−1.3)	725.8 (−2.2)	728.0	(oop) CH_2 A bend
ν_9	A′	484.7 (1.3)	478.7 (−4.7)	482.2 (−1.2)	481.6 (−1.8)	483.4	C=CF bend
MAE[c]		4.2	8.7	2.0	3.5	0.0	

[a]Differences with respect to the CCSD(T)/AVQZ+CV level are reported in parenthesis.
[b]A and S refer to Asymmetric and Symmetric modes, respectively, oop refers to out of plane bending modes.
[c]The Mean Absolute Error (MAE) for each basis set has been calculated by summing the absolute errors on each mode.

to the highest level of theory (i.e., CCSD(T)/AVQZ+CV) are also listed. We observe that for the halo-methane, CH_2F_2, the harmonic frequencies at the CCSD(T)/cc-pVTZ level have an overall Mean Absolute Error (MAE) of 8.7 cm^{-1}, with the largest deviations on the CH stretching modes (about −12 cm^{-1} for ν_6), CH_2 bending modes (about 13 cm^{-1} for ν_8), and one of the CF stretching modes (about 23 cm^{-1} for ν_9). When the diffuse functions are added to the cc-pVTZ basis set, the harmonic frequencies are much closer to the CCSD(T)/AVQZ+CV results, showing an overall MAE of 6.2 cm^{-1}, and errors on ν_6, ν_8, and ν_9 reduced to about −9, −4, and −6 cm^{-1}, respectively. More in general, for almost all modes the harmonic frequencies calculated with the cc-pVTZ basis set are overestimated with respect to the reference calculations, and the effect of the diffuse functions is to lower their absolute values, thus reducing the magnitude of the discrepancies below 10 cm^{-1}.

For CH_2CHF, which is the simplest halo-ethylene among those studied in this work, the frequencies at the CCSD(T)/cc-pVTZ level show an overall MAE of only 4.2 cm^{-1} with respect to the CCSD(T)/AVQZ+CV calculations, and in most cases they are underestimated. The inclusion of diffuse functions to the triple-ζ basis set in most of cases causes a further lowering of the frequency values, resulting in an overall MAE for the CCSD(T)/aug-cc-pVTZ calculations of 8.7 cm^{-1}, thus doubled with respect to CCSD(T)/cc-pVTZ. In particular, deviations of about 10 cm^{-1} are found at the CCSD(T)/AVTZ level for the frequencies of the normal modes involving a distortion of the π bond – such as the C=C stretching (ν_4) and the out of plane bendings (ν_{10} and ν_{11}) – while for the same modes the errors are smaller than 5 cm^{-1} at the CCSD(T)/cc-pVTZ level.

The MAEs reported in Tables II and III have been plotted in Figure 1 for a better visualization. From Figure 1 it is apparent that the harmonic frequencies of CH_2F_2 converge linearly and monotonically along the proposed series of basis sets (VTZ, AVTZ, VQZ, AVQZ). When moving from CCSD(T)/AVQZ to the CCSD(T)/AVQZ+CV level, we note an increase of the slope due to the different nature of the correction. On the other side, for CH_2CHF the calculations do not converge monotonically, and the harmonic frequencies obtained with basis sets employing diffuse functions have a faster convergence but with higher MAEs, when compared with the same basis set without diffuse functions. This can be related to the fact that for halo-methanes only σ bonds occur and polarization effects induced by halogens only affect the σ charge distribution, leading to a linear convergence of the harmonic frequencies. In halo-ethylenes, the π charge distribution introduces another degree of complexity, so that the addition of diffuse functions to the triple-ζ basis results in a lower accuracy of the CCSD(T)/aug-cc-pVTZ harmonic frequencies with respect to their CCSD(T)/cc-pVTZ

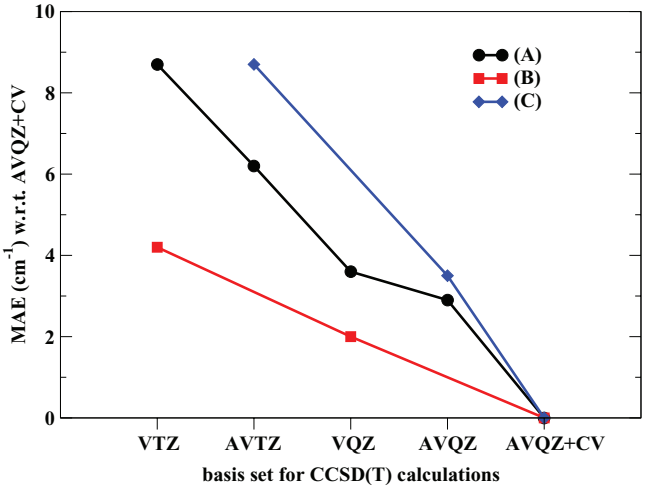

FIG. 1. Mean absolute errors (cm^{-1}) of the fundamental harmonic frequencies computed at the CCSD(T) level employing different basis sets, with respect to CCSD(T)/AVQZ+CV results (see text for details). VTZ, AVTZ, VQZ, and AVQZ mean the cc-pVTZ, aug-cc-pVTZ, cc-pVQZ, and aug-cc-pVQZ basis sets, respectively. CV denotes core-valence correlation corrections (CCSD(T)/cc-pCVTZ). (A) Convergence of calculations for CH_2F_2. (B) Convergence of calculations for CH_2CHF without diffuse functions. (C) Convergence of calculations for CH_2CHF employing diffuse functions.

counterparts. As a final remark, we note that the CV corrections increase the harmonic frequencies by about 1–5 cm^{-1}.

In Tables S.I and S.II in the supplementary material,[92] the harmonic intensities computed at the same levels as discussed above for frequencies are collected for the fundamental modes of CH_2F_2 and CH_2CHF, respectively. In analogy with the results obtained for frequencies, we find that for difluoromethane the inclusion of diffuse functions in the triple-ζ basis set leads to a significant improvement of the results, thus reducing the overall error on the intensities from about 6 km/mol to less than 1 km/mol with respect to CCSD(T)/AVQZ+CV. On the other side, for CH_2CHF the improvement of the intensities due to the inclusion of the diffuse functions in the triple-ζ basis set is quite small, the overall MAE only reducing from 2.13 km/mol with cc-pVTZ to 1.55 km/mol. This suggests that for the halo-ethylenes, the use of the aug-cc-pVTZ basis set for the calculation of infrared spectra leads to a small refinement of the intensities with respect to employment of cc-pVTZ, at the price of a sensibly lower accuracy for frequencies.

Following these arguments, we chose as basis sets in the reference CCSD(T) calculations (CCSD(T)/REF hereafter) for the heavier molecules the aug-cc-pVTZ basis set for halo-methanes, and cc-pVTZ for halo-ethylenes. In Table I, a summary of the CCSD(T)/REF levels for each molecule is reported. In all cases, when the bromine and iodine elements are present, pseudopotentials have been included to describe core electrons (see Sec. II B). The effects of the inclusion of such pseudopotentials on vibrational properties have been quantified by the comparison with the corresponding all-electron basis sets for the molecules containing bromine (for bromine, the all-electron cc-pVTZ and aug-cc-pVTZ basis sets are available, which is not the case for iodine), and in all cases the deviations between all-electron and pseudopotential calculations have been found smaller than 5 cm^{-1} for harmonic frequencies and than 5% for harmonic intensities of the fundamental modes. For iodine, even if not verified by analogous comparison, larger effects are expected. We only note that, for example, for electric first-order properties the extent of relativistic effects enlarges from being about 4%–5% for Br to about 16%–17% for I.[87]

B. Geometries and fundamental frequencies

In Table IV, the DFT bond lengths are compared to their CCSD(T)/REF counterparts and the MAEs with respect to the reference geometries are evaluated for each molecule. In Table S.III in the supplementary material,[92] an analogous comparison has been reported for valence angles. For bond lengths, the MAEs associated to the DFT methods are about 0.007 Å for B3LYP/SNSD and 0.003 Å for B2PLYP/cc-pVTZ(-PP), while for angles in all cases the discrepancies are smaller than 1°, thus suggesting that on average both approaches provide geometries in reasonably good agreement with the reference coupled-cluster results.

In Table V, the MAEs of the anharmonic frequencies with respect to the experimental data are reported for the whole set of molecules. Detailed data for each molecule, including harmonic and anharmonic frequencies, errors for each mode, Fermi resonances, assignments of the transitions, and comparison with other computational results available in literature are collected in Tables S.IV– S.IX in the supplementary material.[92] $CHBrF_2$ and CF_2CFCl have been chosen

TABLE IV. Bond lengths and Mean Absolute Errors (MAEs) with respect to CCSD(T)/REF. Values in Å.[a]

	B3LYP/ SNSD	B2PLYP/ cc-pVTZ(-PP)	CCSD(T)/ REF
	CH_2F_2		
C–H	1.0942	1.0878	1.0877
C–F	1.3656	1.3576	1.3542
	$CHBrF_2$		
C–H	1.0909	1.0843	1.0870
C–F	1.3448	1.3383	1.3417
C–Br	1.9554	1.9446	1.9360
	CF_3Br		
C–Br	1.9453	1.9357	1.9285
C–F	1.3330	1.3266	1.3276
	CH_2DBr		
C–Br	1.9628	1.9472	1.9471
C–H(D)	1.0887	1.0823	1.0857
	CH_2CHF		
C–F	1.3515	1.3439	1.3431
C=C	1.3254	1.3197	1.3233
C–H(c)	1.0853	1.0784	1.0788
C–H(g)	1.0861	1.0797	1.0801
C–H(t)	1.0843	1.0773	1.0788
	CF_2CFCl		
C=C	1.3316	1.3260	1.3319
C–F(g)	1.3342	1.3312	1.3305
C–F(t)	1.3199	1.3151	1.3137
C–F(c)	1.3182	1.3134	1.3137
C–Cl	1.7209	1.7072	1.7089
	cis-CHFCHBr		
C–Br	1.8881	1.8787	1.8815
C=C	1.3283	1.3228	1.3309
C–F	1.3402	1.3342	1.3339
C–H(Br)	1.0826	1.0758	1.0782
C–H(F)	1.0862	1.0799	1.0818
	cis-CHFCHI		
C–I	2.0986	2.0821	2.0875
C=C	1.3274	1.3225	1.3308
C–F	1.3414	1.3355	1.3351
C–H(I)	1.0826	1.0763	1.0788
C–H(F)	1.0870	1.0806	1.0825
	Overall MAEs[b]		
Halo-methanes (9)	0.0095	0.0033	0.0000
Halo-ethylenes (20)	0.0054	0.0025	0.0000
Total (29)	0.0067	0.0028	0.0000
C–H (10)	0.0048	0.0017	0.0000
C=C (4)	0.0021	0.0064	0.0000
C–F (9)	0.0061	0.0013	0.0000
C–Cl (1)	0.0120	0.0017	0.0000
C–Br (4)	0.0146	0.0047	0.0000
C–I (1)	0.0110	0.0055	0.0000

[a](c), (g), and (t) stand for cis-, geminal-, and trans-, respectively.

[b]Overall MAEs are computed by averaging the errors of the bond lengths over all halo-methanes, halo-ethylenes, and the whole set of molecules (total). The number of non-equivalent bonds considered in the calculation of the MAEs is given in parenthesis.

TABLE V. Mean absolute errors (cm^{-1}) for the anharmonic (GVPT2) frequencies of the fundamental modes with respect to the experimental frequencies.[a]

	B3LYP/ SNSD	B2PLYP/ VTZ[b]	HYB^{B3D}[c]	HYB^{B2T}[d]
CH_2F_2	28.8	6.9	4.9	2.7
$CHBrF_2$	23.1	6.9	2.3	3.1
CF_3Br	26.0	9.8	3.5	3.5
CH_2DBr	9.9	7.3	4.4	4.0
CH_2CHF	8.5	11.6	3.2	2.9
CF_2CFCl	12.5	7.2	9.1	8.4
cis-CHFCHBr	8.0	8.2	4.3	3.7
cis-CHFCHI	8.0	8.0	4.6	3.6
Halo-methanes (33)	22.0	7.7	3.8	3.3
Halo-ethylenes (48)	9.3	8.8	5.3	4.7
Total (81)	14.7	8.3	4.6	4.1
C–H st. (13)	8.8	13.9	5.1	4.6
C–F st. (11)	32.0	9.2	8.5	8.3
C–Cl st. (1)	8.2	1.0	2.4	1.9
C–Br st. (4)	20.4	6.3	2.0	2.6
C–I st. (1)	18.6	0.4	1.3	1.4

[a]See the supplementary material for details about the frequencies of each molecule. The number of modes considered in the calculation of the MAEs is given in parenthesis.
[b]cc-pVTZ (cc-pVTZ-PP for Br and I).
[c]Anharmonic shifts at the B3LYP/SNSD level summed to the CCSD(T)/REF harmonic frequencies. See text, Sec. II D.
[d]Anharmonic shifts at the B2PLYP/cc-pVTZ(-PP) level summed to the CCSD(T)/REF harmonic frequencies. See text, Sec. II D.

as case studies; therefore, the corresponding tables will be reported and discussed in dedicated sections, while in the following a general discussion is presented. First of all, we note that the overall MAE of the B3LYP/SNSD level is about 15 cm^{-1}, which is comparable with previous results, obtained, for example, for glycine[44] and uracil[59] (MAEs of about 10 cm^{-1} in both cases). The slightly larger errors found in the present case are related to the presence of the halogen atoms, which introduce further degrees of complexity due to the large electronegativity and – for the heavy-atom-containing compounds – to the relativistic effects. In particular, we observe that the frequencies of the C–F, C–Br, and C–I stretchings are affected by the largest errors (about 30 cm^{-1} for C–F and 20 cm^{-1} for C–Br and C–I), which are the origin of the large MAEs observed for CH_2F_2 (29 cm^{-1}), $CHBrF_2$ (23 cm^{-1}), and CF_3Br (26 cm^{-1}). The errors on the frequencies for modes associated to the chlorine atom are rather limited, being only 8 cm^{-1} for the C–Cl stretching mode of CF_2CFCl. Overall better performances are observed in B2PLYP/cc-pVTZ(-PP) computations, with a mean error on the frequencies of the C–F stretching modes of only 9 cm^{-1}, and MAEs of about 1 cm^{-1} for C–Cl and C–I and 6 cm^{-1} for the C–Br stretchings. On the whole, this leads to overall MAEs smaller than 10 cm^{-1} for the fundamental frequencies of CH_2F_2, $CHBrF_2$, and CF_3Br. Therefore, the use of a triple-ζ basis set and the inclusion of a fraction of the MP2 energy leads to a noticeable improvement of the anharmonic frequencies with respect to the B3LYP/SNSD results, thus suggesting that the polarization effects induced by the large electronegativity of the fluorine atoms can be accurately accounted for with a triple-ζ basis set. Nevertheless, the B3LYP/SNSD approach remains a valuable alternative for open-shell systems or for very large molecules, for which the B2PLYP/cc-pVTZ method is much more prone to spin contamination errors and/or much more computationally demanding. In the test cases discussed in Sec. III D, the harmonic and anharmonic frequencies computed at the B3LYP/cc-pVTZ(-PP) level are reported in order to separate the effects of the functional and the basis set contributing to the enhanced accuracy of the B2PLYP/cc-pVTZ(-PP) frequencies with respect to the B3LYP/SNSD ones.

A possible route to correct for a large fraction of error in the computed vibrational frequencies is based on the hybrid approach described in detail in Sec. II D, and already used in previous works.[53–60] For the molecules investigated here, such an approach has the noticeable advantage that the treatment at the CCSD(T) level of the harmonic terms allows to better take into account the large electronegativity of halogens and the relativistic effects on Br and I. The hybrid frequencies for each molecule, calculated by combining the harmonic frequencies at the CCSD(T)/REF level with the cubic and semi-diagonal quartic force constants at the B3LYP/SNSD level (HYB^{B3D}) and at the B2PLYP/cc-pVTZ (-PP) level (HYB^{B2T}), are reported in Tables S.IV– S.IX (supplementary material),[92] VII and IX, while in Table V the MAEs with respect to the corresponding experimental frequencies are collected. The largest errors found for the HYB^{B3D} frequencies are again related to the C–F stretching modes, but in this case the overall MAE is only 8 cm^{-1}. Such an improved accuracy, with respect to the B3LYP/SNSD computations, can be also observed for the frequency modes involving chlorine, bromine, and iodine, and it can be ascribed to the fact that the inaccuracies due to the presence of the halogens have been corrected at the harmonic level by the CCSD(T)/REF calculations, thus leading to a total MAE, averaged over all molecules, of only 4.6 cm^{-1}. These beneficial effects are also evident when comparing the B2PLYP/cc-pVTZ(-PP) frequencies (total MAE of 8 cm^{-1}) with the HYB^{B2T} frequencies (4 cm^{-1}). Furthermore, it is worth noting that the correction of the harmonic part at the CCSD(T) level turns out to be more important for B3LYP/SNSD than for B2PLYP/cc-pVTZ(-PP), due to the already noticeable accuracy of the latter. This is graphically shown in Figure 2, where the signed errors for the B3LYP/SNSD and B2PLYP/cc-pVTZ(-PP) harmonic frequencies with respect to the CCSD(T)/REF ones, for the 81 modes of the molecules considered, are plotted versus the CCSD(T)/REF frequencies. From this figure, we observe that the error distribution of the B2PLYP/cc-pVTZ(-PP) harmonic frequencies is much narrower than that for B3LYP/SNSD, the former being mostly within 10 cm^{-1}. This suggests that hybrid approaches similar to those used in previous works,[44,50] in which the harmonic frequencies are computed at the B2PLYP/cc-pVTZ(-PP) level and the anharmonic shifts at the B3LYP/SNSD level – i.e., not requiring coupled-cluster computations – can be safely used for large molecules containing halogens, and the accuracy of such frequencies should be very close to that of the HYB^{B3D} method. In Figure 2, we also note that the frequencies at the B3LYP/SNSD level are mostly overestimated in the 3000–4000 cm^{-1} range, mostly underestimated in the zone between

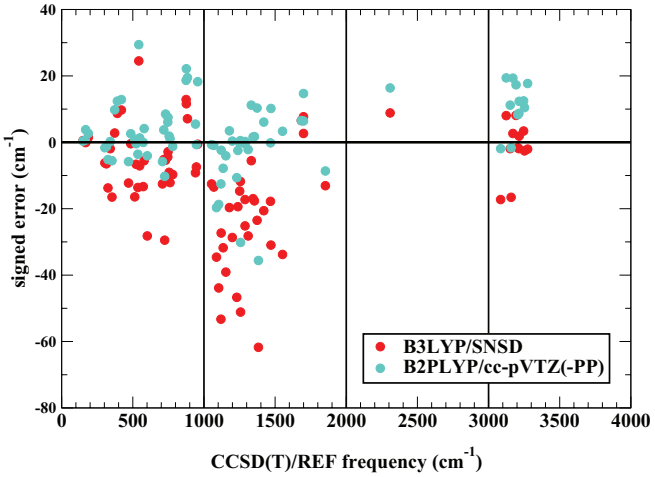

FIG. 2. Signed errors (cm^{-1}) of the B3LYP/SNSD and B2PLYP/cc-pVTZ (-PP) harmonic frequencies with respect to CCSD(T)/REF calculations.

1000 and 2000 cm^{-1}, while the errors are scattered in the region below 1000 cm^{-1}. This suggests that the discrepancies at the B3LYP/SNSD level are related to an intrinsic limit of the DFT/double-ζ calculations and that it is not possible to derive a single empirical scaling factor able to correct the frequencies of all the fundamental modes.

The improvement due to CCSD(T) on the peak positions in the IR spectra is graphically pointed out by means of some representative vibrations of one halo-methane in Figure 3 and one halo-ethylene in Figure 4. In Figure 3, the IR spectrum of the $CHBrF_2$ molecule has been plotted in the CH stretching frequency range (2980–3060 cm^{-1}). The frequencies have been computed at the B3LYP/SNSD level (DFT/DFT) and also with the HYB^{B3D} approach (HYB/DFT), while the DFT intensities have been normalized to unitary values, since a detailed discussion of the absorption cross sections is postponed to Sec. III C. In Figure 4, the CCF and CCH bending zone of the cis-CHFCHBr molecule (700–760 cm^{-1}) is shown,

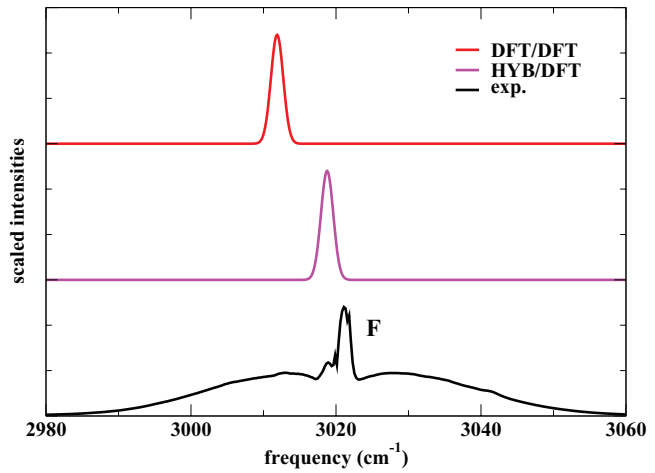

FIG. 3. Infrared spectrum of $CHBrF_2$ in the CH stretching frequency range. The label F of the peak is consistent with Figure 8. A FWHM of 2 cm^{-1} has been used for the convolution. DFT calculations at the B3LYP/SNSD level. Note that the experimental line shape is due to the rotational structure of the vibrational band, while this has not been considered in the theoretical spectrum.

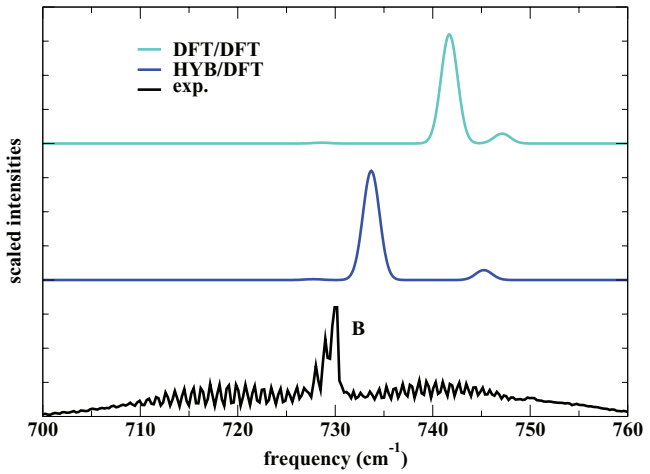

FIG. 4. Infrared spectrum of cis-CHFCHBr in the CCF and CCH bending modes frequency range. The label B of the peak is consistent with Figure 5. A FWHM of 2 cm^{-1} has been used for the convolution. DFT calculations at the B2PLYP/cc-pVTZ-PP level. Note that the experimental line shape is due to the rotational structure of the vibrational band, while this has not been considered in the theoretical spectrum.

the frequencies being obtained at the B2PLYP/cc-pVTZ-PP (DFT/DFT) and HYB^{B2T} (HYB/DFT) levels. In both figures, the beneficial effect of the CCSD(T) corrections to the harmonic frequencies on the peak positions can be observed. It is worth noting that an accurate reproduction of the peak position is also of paramount importance for a quantitative comparison of the integrated cross sections with the experimental data, since they determine the correct choice of the transitions to be included in a given frequency range.

C. Intensities

For CH_2F_2, $CHBrF_2$, CF_3Br, CH_2CHF, and CF_2CFCl, experimental absorption cross sections (cm^2/molecule) are available, and their integration over selected frequency ranges leads to integrated cross sections (km/mol), which can be directly related to the computed values (see Sec. II A). For $CHBrF_2$ and CF_2CFCl the discussion and the corresponding tables are reported in a separate section, while in Tables S.X–S.XII in the supplementary material[92] the comparison between experimental and theoretical integrated cross sections is reported for the remaining three molecules mentioned above. A summary of the MAEs of the computed integrated cross sections with respect to experiment is given in Table VI. We observe that for both proposed DFT methods the agreement between theoretical and experimental intensities is very good, the total MAE being about 7 km/mol for B3LYP/SNSD and 6 km/mol for B2PLYP/cc-pVTZ(-PP). On average, both methods provide very similar intensity values, thus suggesting that electrostatic properties, such as the dipole moment of the ground state, should also be in close agreement and that the effect of the double-/triple-ζ basis sets should be smaller than that observed for frequencies. Furthermore, a similar accuracy is found for both halo-methanes (MAEs of about 6 km/mol for both B3LYP/SNSD and B2PLYP/cc-pVTZ(-PP)) and halo-ethylenes (MAE of about 8 km/mol for B3LYP/SNSD and about 5 km/mol for B2PLYP/cc-pVTZ(-PP)) because infrared

TABLE VI. Mean absolute errors (km/mol) for the integrated absorption cross sections with respect to the experimental data.[a]

	B3LYP/ SNSD	B2PLYP/ VTZ[b]	HYB^{B3D}[c]	HYB^{B2T}[d]
CH_2F_2	3.40	3.22	1.98	1.71
$CHBrF_2$	6.55	6.18	1.99	1.93
CF_3Br	8.21	9.78	2.37	2.29
CH_2CHF	11.05	7.57	5.02	5.07
CF_2CFCl	4.82	3.16	1.47	1.39
Halo-methanes	6.05	6.39	2.11	1.98
Halo-ethylenes	7.94	5.37	3.25	3.23
Total	6.81	5.98	2.57	2.48

[a]Anharmonic intensities of overtones and combination bands have been included. See the supplementary material for details about each molecule.
[b]cc-pVTZ (cc-pVTZ-PP for Br and I).
[c]B3LYP/SNSD intensities empirically corrected with the CCSD(T)/REF harmonic intensities of the fundamental modes. See text, Sec. II D.
[d]B2PLYP/cc-pVTZ(-PP) intensities empirically corrected with the CCSD(T)/REF harmonic intensities of the fundamental modes. See text, Sec. II D.

intensities are less sensitive to the molecular geometry than frequencies, being lower-order derivatives with respect to atomic displacements, thus suggesting that the performances of the methods should be quite similar for a large set of molecular systems. In the last two columns of Table VI, the hybrid IR intensities at the HYB^{B3D} and HYB^{B2T} levels are reported. For the details about the hybrid approach for the integrated cross sections, we refer to Sec. II D, while here we only point out that from the MAEs associated to both the hybrid data sets (smaller than 2 km/mol) it is evident that hybrid approaches are useful in order to improve the theoretical intensities.

For cis-CHFCHBr, cis-CHFCHI, and CH_2DBr, the experimental data are available in units of absorbance. In this case, a quantitative comparison between experimental and theoretical spectra is not possible, since the information about the optical length of the instrument and the concentration/partial pressure of the samples were not known at the moment of the measure with the required accuracy. Nevertheless, useful information can be extracted from a qualitative comparison between experimental and theoretical IR spectra. In Figure 5, the experimental IR spectrum in absorbance units of cis-CHFCHBr has been normalized with respect to the most intense peak, so that the latter (peak C) takes an unitary value. On the other side, the calculated integrated cross sections have been first convoluted with Gaussian functions (FWHM = 20 cm^{-1}), then scaled in analogous manner, in order to allow a direct comparison between DFT and experimental spectra. On average, although the peak positions in Figure 5 are well reproduced already at the B2PLYP/cc-pVTZ-PP level, in agreement with the results shown in Table V and discussed in Sec. III B, further improvements are noted when

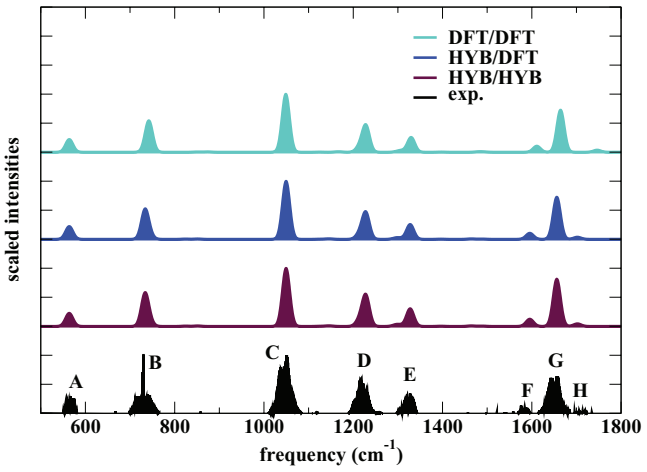

FIG. 5. Infrared spectrum of cis-CHFCHBr, as calculated with pure DFT approach (DFT/DFT), hybrid coupled-cluster and DFT approach for frequencies only (HYB/DFT), hybrid coupled-cluster and DFT approach for frequencies and intensities (HYB/HYB). DFT calculations at the B2PLYP/cc-pVTZ-PP level, HYB calculations employ harmonic corrections at the CCSD(T)/REF level. A FWHM of 20 cm^{-1} has been used for the convolution. (A) CBr stretching. (B) CCF and CCH symmetric out of plane bendings. (C) CF stretching. (D) CHBr and CHF symmetric in plane bendings. (E) CHBr and CHF asymmetric in plane bendings. (F) Overtones and combination bands. (G) CC stretching. (H) Overtones and combination bands.

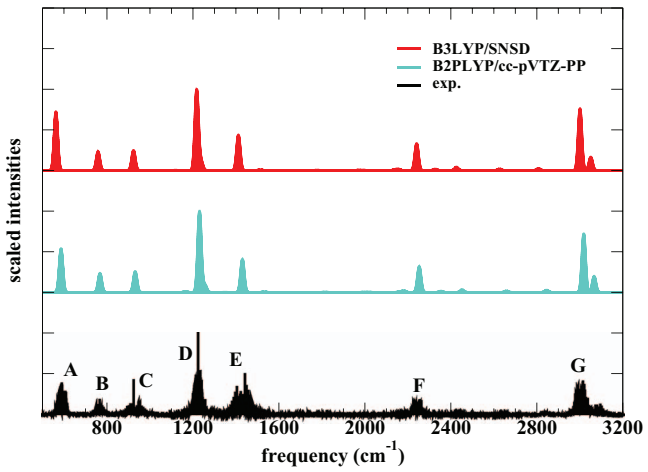

FIG. 6. Infrared spectrum of CH_2DBr. A FWHM of 20 cm^{-1} has been used for the convolution. (A) CBr stretching. (B) DCBr deformation. (C) CH_2 rock. (D) CH_2 twist and wag. (E) CH_2 deformation. (F) CD stretching. (G) CH_2 asymmetric and symmetric stretchings.

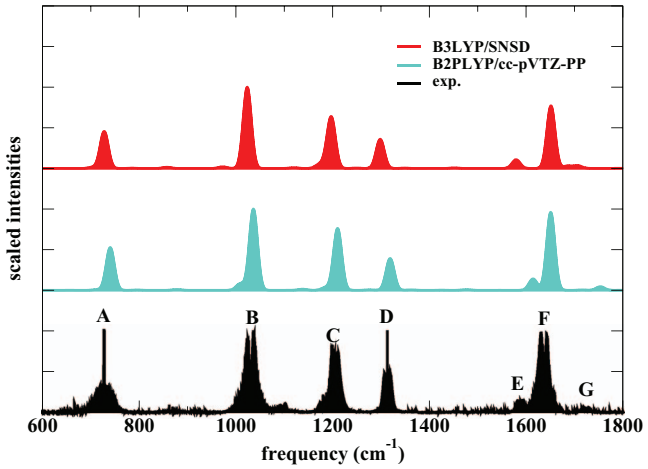

FIG. 7. Infrared spectrum of cis-CHFCHI. A FWHM of 20 cm^{-1} has been used for the convolution. (A) CCF and CHI out of plane bending. (B) CF stretching. (C) CHI/CHF symmetric in plane bending. (D) CHI/CHF asymmetric in plane bending. (E) Overtones and combination bands of CCF bending. (F) CC stretching. (G) Overtones and combination bands of CHI out of plane bendings.

TABLE VII. Harmonic and anharmonic (GVPT2) frequencies (cm^{-1}) of $CHBrF_2$.

Harmonic frequencies[a]							
Modes	Symm.	B3LYP/ SNSD	B3LYP/ cc-pVTZ-PP	B2PLYP/ cc-pVTZ-PP	CCSD(T)/ F-AVTZ[b,c]	CCSD(T)/ REF	Assignments[d]
ν_1	A′	3149.3 (−1.9)	3129.3 (−21.9)	3162.4 (11.2)	3155.8 (4.6)	3151.2	CH stretch
ν_7	A″	1350.5 (−23.5)	1369.6 (−4.4)	1384.3 (10.3)	1373.7 (−0.3)	1374.0	CF_2 twist/CH (oop) bend
ν_2	A′	1282.2 (−28.2)	1288.7 (−21.7)	1308.2 (−2.2)	1312.7 (2.3)	1310.4	CF_2 wag/CH (ip) bend
ν_8	A″	1114.0 (−39.1)	1132.2 (−20.9)	1149.0 (−4.1)	1151.2 (−1.9)	1153.1	CF_2 (A) stretch
ν_3	A′	1093.6 (−27.3)	1106.6 (−14.3)	1118.5 (−2.4)	1119.3 (−1.6)	1120.9	CF_2 (S) stretch
ν_4	A′	694.9 (−29.5)	694.0 (−30.4)	714.1 (−10.3)	724.0 (−0.4)	724.4	HCBr deformation
ν_5	A′	574.5 (−5.5)	579.8 (−0.2)	584.1 (4.1)	580.8 (0.8)	580.0	CF_2 deformation
ν_6	A′	311.3 (−13.7)	310.4 (−14.6)	319.8 (−5.2)	325.7 (0.7)	325.0	CBr stretch
ν_9	A″	307.8 (−6.5)	306.6 (−7.7)	312.9 (−1.4)	313.6 (−0.7)	314.3	CF_2 rock
MAE		19.5	15.1	5.7	1.5	0.0	

Anharmonic frequencies[a]										
Modes	Symm.	B3LYP/ SNSD	B3LYP/ cc-pVTZ-PP	B2PLYP/ cc-pVTZ-PP	HYB^{B3D}[e]	HYB^{B3T}[f]	HYB^{B2T}[g]	CCSD(T)/ F-AVTZ[b,c,h]	Exp.[b]	Assignments[d]
ν_1	A′	3011.9 (−9.0)	3000.3 (−20.6)	3034.2 (13.3)	3018.8 (−2.1)	3026.3 (5.4)	3021.1 (0.2)	3023.2 (2.3)	3020.9	CH stretch
ν_7	A″	1318.9 (−27.7)	1336.9 (−9.7)	1351.0 (4.4)	1343.8 (−2.8)	1342.1 (−4.5)	1340.6 (−6.0)	1340.8 (−5.8)	1346.6	CF_2 twist/CH (oop) bend
ν_2	A′	1254.4 (−27.4)	1259.5 (−22.3)	1279.6 (−2.2)	1284.2 (2.4)	1282.9 (1.1)	1282.1 (0.3)	1282.5 (0.7)	1281.8	CF_2 wag/CH (ip) bend
ν_8	A″	1085.7 (−45.1)	1105.0 (−25.9)	1121.6 (−9.2)	1128.5 (−2.3)	1127.7 (−3.1)	1126.0 (−4.8)	1125.6 (−5.2)	1130.8	CF_2 (A) stretch
ν_3	A′	1069.6 (−33.2)	1083.1 (−19.7)	1094.8 (−8.0)	1099.7 (−3.1)	1098.9 (−3.9)	1097.3 (−5.5)	1096.3 (−6.5)	1102.8	CF_2 (S) stretch
ν_4	A′	687.1 (−31.6)	686.1 (−32.6)	705.6 (−13.1)	717.7 (−1.0)	717.7 (−1.0)	716.4 (−2.3)	715.6 (−3.1)	718.7	HCBr deformation
ν_5	A′	567.2 (−11.8)	572.2 (−6.8)	576.6 (−2.4)	573.4 (−5.6)	573.0 (−6.0)	572.6 (−6.4)	572.7 (−6.3)	579.0	CF_2 deformation
ν_6	A′	308.1 (−15.2)	307.3 (−16.0)	316.3 (−7.0)	322.3 (−1.0)	322.5 (−0.8)	321.7 (−1.6)	321.7 (−1.6)	323.3	CBr stretch
ν_9	A″	305.4 (−7.3)	303.9 (−8.8)	310.0 (−2.7)	312.0 (−0.7)	311.8 (−0.9)	311.5 (−1.2)	313.2 (0.5)	312.7	CF_2 rock
MAE		23.1	18.0	6.9	2.3	3.0	3.1	3.6	0.0	

[a]In parenthesis, the absolute errors are reported. Errors of harmonic frequencies have been computed with respect to the CCSD(T)/REF harmonic frequencies, errors of anharmonic frequencies evaluated with respect to experimental fundamentals. Mean Absolute Errors (MAEs) have been derived by averaging over the errors of each mode. No Fermi resonances found for this molecule.
[b]Pietropolli Charmet *et al.*[18]
[c]cc-pVTZ for H, C, Br, aug-cc-pVTZ for fluorine.
[d](A) and (S) refer to, respectively, Asymmetric and Symmetric modes, (ip) and (oop) refer to, respectively, in plane and out of plane bending mode.
[e]Harmonic frequencies at the CCSD(T)/REF level, cubic and semi-diagonal quartic force constants at the B3LYP/SNSD level.
[f]Harmonic frequencies at the CCSD(T)/REF level, cubic and semi-diagonal quartic force constants at the B3LYP/cc-pVTZ-PP level.
[g]Harmonic frequencies at the CCSD(T)/REF level, cubic and semi-diagonal quartic force constants at the B2PLYP/cc-pVTZ-PP level.
[h]CCSD(T)/F-AVTZ geometry and second-order force constants, CCSD(T)/cc-pVTZ third- and fourth-order force constants.

incorporating the CCSD(T) corrections either to frequencies only (HYB/DFT) or to both frequencies and intensities (HYB/HYB). For example, a sensible improvement of the frequency of peak H, associated to overtones and combination bands of the low frequency modes, is observed when going from DFT/DFT to the HYB/DFT spectra. In this regard, it should be pointed out that the CCSD(T)/REF corrections to frequencies are applied to all bands, also including overtones, while the corrections to harmonic intensities influence only the fundamental transitions.

In Figures 6 and 7, the IR spectra of CH_2DBr and cis-CHFCHI, respectively, at the B3PLYP/SNSD and B2PLYP/cc-pVTZ-PP levels are compared with the experimental spectra by applying the scaling procedure described above to the experimental absorbance and computed spectral line shape. Even for these non-trivial molecules, where iodine and isotopic substitutions are involved, the intensities calculated at the DFT levels are very close to the experimental data, and this is particularly evident in peak F of Figure 6, related to the C–D stretching of CH_2DBr, and peaks A, C, D, G of Figure 7, related to the modes involving iodine.

D. Test cases: The IR spectra of the $CHBrF_2$ and CF_2CFCl

In this section, we report a detailed discussion on the computation of the full IR spectra of $CHBrF_2$ and CF_2CFCl, which have been chosen as test cases for halo-methanes and halo-ethylenes, respectively, due to their importance from an environmental point of view[88–90] and to the availability of experimental intensities in cross section units. In particular, $CHBrF_2$ was initially proposed as an interim replacement to fully halogenated halons, being subsequently phased out by the Copenhagen amendment of the Montreal protocol.

In Table VII, the frequencies of $CHBrF_2$ computed at the B3LYP/SNSD, B2PLYP/cc-pVTZ-PP, and B3LYP/cc-pVTZ

TABLE VIII. Integrated cross sections (km/mol) of $CHBrF_2$.

Harmonic integrated cross sections				
Range (cm^{-1})	Main transitions	B3LYP/ SNSD	B2PLYP/ cc-pVTZ	CCSD(T)/ REF
530–610	ν_5	5.58	5.80	4.94
610–660	$2\nu_6$	...	...	...
670–750	ν_4	125.49	120.40	103.00
1050–1190	ν_3,ν_8	495.24	480.33	449.76
1240–1310	ν_2	70.44	85.79	80.89
1310–1460	ν_7,$2\nu_4$	7.26	12.05	10.66
1650–1700	$\nu_3+\nu_5$	...	...	...
1950–2300	$2\nu_3$,$2\nu_8$,$\nu_3+\nu_8$	...	...	...
2350–2720	$2\nu_2$,$2\nu_7$	...	...	...
2950–3100	ν_1	5.46	11.34	6.50
3700–3800	$\nu_1+\nu_4$	...	...	...
4050–4200	$\nu_1+\nu_3$	...	...	...
4260–4380	$\nu_1+\nu_2$	...	...	...
5870–5980	$2\nu_1$	...	...	...
MAE[a]		13.92	9.99	0.00

Anharmonic integrated cross sections						
Range (cm^{-1})	Main transitions	B3LYP/ SNSD	B2PLYP/ cc-pVTZ	HYB^{B3D}[b]	HYB^{B2T}[c]	Exp.[d]
530–610	ν_5	5.53	5.70	4.89	4.85	5.1(1)
610–660	$2\nu_6$	1.41	1.41	1.41	1.41	1.904(6)
670–750	ν_4	126.35	120.77	103.86	103.37	101.8(5)
1050–1190	ν_3,ν_8	480.49	467.20	435.02	436.63	421.1(1)
1240–1310	ν_2	69.92	84.27	80.37	79.37	72.4(2)
1310–1460	ν_7,$2\nu_4$	7.11	11.43	10.52	10.05	9.9[e]
1650–1700	$\nu_3+\nu_5$	0.73[f]	0.78	0.73[f]	0.78	0.73(2)
1950–2300	$2\nu_3$,$2\nu_8$,$\nu_3+\nu_8$	7.72	7.69	7.72	7.69	7.3(1)
2350–2720	$2\nu_2$,$2\nu_7$	1.10	1.28	1.10	1.28	1.25(2)
2950–3100	ν_1	7.74	13.65	8.78	8.81	7.71(6)
3700–3800	$\nu_1+\nu_4$	0.21	0.23	0.21	0.23	0.27(2)
4050–4200	$\nu_1+\nu_3$	0.61	0.65	0.61	0.65	0.61(1)
4260–4380	$\nu_1+\nu_2$	0.54	0.47	0.54	0.47	0.71(1)
5870–5980	$2\nu_1$	1.33	0.87	1.33	0.87	0.66(4)
MAE[g]		6.55	6.18	1.99	1.93	0.00

[a]MAE of harmonic calculations evaluated with respect to the CCSD(T)/REF data.
[b]Harmonic intensities of fundamental modes empirically corrected at the CCSD(T)/AVTZ-PP level, B3LYP/SNSD intensities for all other modes.
[c]Harmonic intensities of fundamental modes empirically corrected at the CCSD(T)/AVTZ-PP level, B2PLYP/cc-pVTZ intensities for all other modes.
[d]Experimental intensities are taken from Pietropolli Charmet *et al.*[18]
[e]The 1310–1400 and 1400–1460 cm^{-1} ranges have been merged in order to facilitate the assignments.
[f]Although the frequency of the ($\nu_3+\nu_5$) combination band is 1631.7 cm^{-1} at the B3LYP/SNSD level, it has anyway been included in the 1650−1700 cm^{-1} range for consistency with the experimental assignment.
[g]MAE of anharmonic calculations evaluated with respect to the experimental data.

-PP levels as well as employing hybrid approaches are compared with the reference CCSD(T) data and experimental results. The errors of the harmonic and anharmonic frequencies have been evaluated with respect to the CCSD(T)/REF calculations and experimental fundamentals, respectively. The harmonic frequencies calculated at the CCSD(T)/REF level in this work are in very close agreement with the results by Pietropolli Charmet *et al.*,[18] obtained at a similar level of theory (they included diffuse functions only on the fluorine atom, while we performed the calculations with the complete aug-cc-pVTZ-PP basis set), with an overall MAE of 1.5 cm^{-1}. The MAE of the DFT harmonic frequencies is about 20 cm^{-1} for B3LYP/SNSD and about 6 cm^{-1} for B2PLYP/cc-pVTZ-PP, in line with the results presented in Table V and Figure 2. Furthermore, concerning the MAE of the B3LYP/cc-pVTZ-PP frequencies (15 cm^{-1}), we note an improvement of about 5 cm^{-1} with respect to the B3LYP/SNSD level, and a difference of about 10 cm^{-1} with respect to B2PLYP/cc-pVTZ-PP, thus suggesting that both the functional and the basis set contribute to the overall accuracy of the DFT frequencies. In the lowest part of Table VII, the comparison between the experimental and anharmonic frequencies is reported for both DFT and hybrid models. The errors associated to the anharmonic frequencies at the DFT level are very similar to what observed for the harmonic frequencies, with a MAE of about 7 and 18 cm^{-1} at the B2PLYP/cc-pVTZ-PP and B3LYP/cc-pVTZ-PP

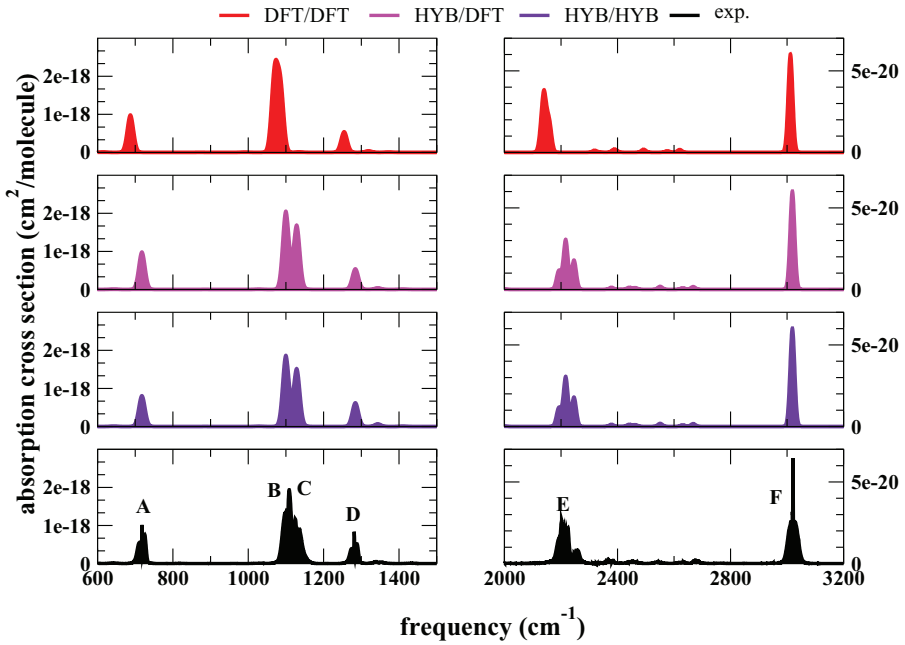

FIG. 8. Infrared spectrum of $CHBrF_2$, as calculated with pure DFT approach (DFT/DFT), hybrid coupled-cluster and DFT approach for frequencies only (HYB/DFT), hybrid coupled-cluster and DFT approach for frequencies and intensities (HYB/HYB). DFT calculations at the B3LYP/SNSD level, HYB calculations employ harmonic corrections at the CCSD(T)/REF level. A FWHM of 20 cm^{-1} has been used for the convolution. (A) HCBr bending. (B) CF_2 symmetric stretching. (C) CF_2 asymmetric stretching. (D) CH in plane and out of planes bendings. (E) Overtones and combination bands of the CF_2 stretching modes. (F) CH stretching. Note that peaks A, B, C, D and E, F are plotted with different scales.

levels, respectively, and of about 23 cm^{-1} for B3LYP/SNSD calculations, the latter reducing to 2.3 cm^{-1} when the hybrid HYB^{B3D} approach is considered. This confirms that a triple-ζ basis set in conjunction with the B2PLYP functional provides results in very good agreement with the CCSD(T)/REF calculations.

In Table VIII, the harmonic integrated cross sections at the B3LYP/SNSD, B2PLYP/cc-pVTZ-PP, and

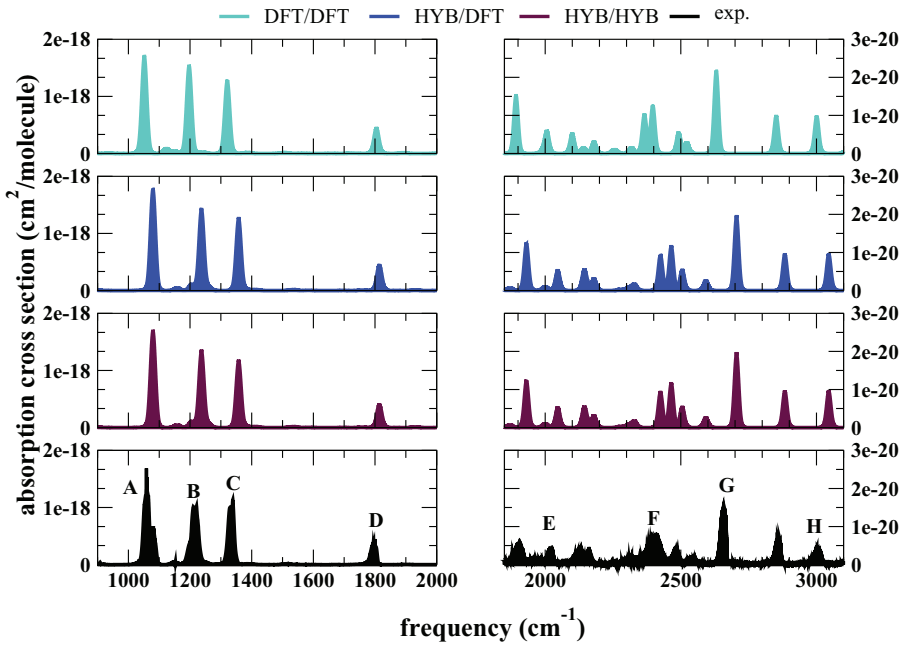

FIG. 9. Infrared spectrum of CF_2CFCl, as calculated with pure DFT approach (DFT/DFT), hybrid coupled-cluster and DFT approach for frequencies only (HYB/DFT), hybrid coupled-cluster and DFT approach for frequencies and intensities (HYB/HYB). DFT calculations at the B2PLYP/cc-pVTZ level, HYB calculations employ harmonic corrections at the CCSD(T)/REF level. A FWHM of 20 cm^{-1} has been used for the convolution. (A) CF_2 symmetric stretching. (B) CF stretching. (C) CF_2 asymmetric stretching. (D) CC stretching. (E) Combination of CF and CCl stretching bands. (F) Overtone of the CF stretching mode, combination of CF_2 symmetric and asymmetric stretching bands. (G) Overtone of the CF_2 symmetric stretching mode. (H) Combination between CC and CF stretching bands. Note that peaks A, B, C, D and E, F, G, H are plotted with different scales.

TABLE IX. Harmonic and anharmonic (GVPT2) frequencies (cm^{-1}) for CF_2CFCl.

Harmonic frequencies[a]							
Modes	Symm.	B3LYP/ SNSD	B3LYP/ cc-pVTZ	B2PLYP/ cc-pVTZ	CCSD(T)/ REF	CCSD(T)/ ANOtz[b]	Assignments[c]
ν_1	A′	1839.7 (−2.3)	1836.7 (−5.3)	1844.2 (2.2)	1852.8 (10.8)	1842.0	C=C stretch
ν_2	A′	1322.4 (−44.6)	1328.6 (−38.4)	1348.6 (−18.4)	1384.2 (17.2)	1367.0	CF_2 (A) stretch
ν_3	A′	1205.0 (−36.0)	1209.1 (−31.9)	1225.9 (−15.1)	1256.1 (15.1)	1241.0	C–F stretch
ν_4	A′	1054.3 (−20.7)	1055.9 (−19.1)	1069.3 (−5.7)	1088.9 (13.9)	1075.0	CF_2 (S) stretch
ν_5	A′	694.7 (−4.3)	696.8 (−2.2)	701.5 (2.5)	707.3 (8.3)	699.0	C–Cl stretch
ν_{10}	A″	567.2 (21.2)	575.7 (29.7)	572.1 (26.1)	542.7 (−3.3)	546.0	(oop) CF_2 wag
ν_6	A′	515.4 (−5.6)	518.6 (−2.4)	521.5 (0.5)	522.0 (1.0)	521.0	CF_2 bend
ν_7	A′	456.9 (−7.1)	458.0 (−6.0)	463.4 (−0.6)	469.2 (5.2)	464.0	F(t)CCF(c) rock
ν_{11}	A″	375.1 (3.1)	380.0 (8.0)	382.1 (10.1)	372.3 (0.3)	372.0	(oop) CFCl wag
ν_8	A′	339.0 (−1.0)	339.8 (−0.2)	341.1 (1.1)	340.9 (0.9)	340.0	CFCl bend
ν_9	A′	188.5 (0.5)	189.6 (1.6)	189.7 (1.7)	187.0 (−1.0)	188.0	CFCl rock
ν_{12}	A″	168.0 (−2.0)	169.7 (−0.3)	171.9 (1.9)	168.1 (−1.9)	170.0	(oop) torsion
MAE		12.4	12.1	7.2	6.6	0.0	

Anharmonic frequencies[a]										
Modes	Symm.	B3LYP/ SNSD	B3LYP/ cc-pVTZ	B2PLYP/ cc-pVTZ	HYB^{B3D}[d]	HYB^{B3T}[e]	HYB^{B2T}[f]	CCSD(T)[b,g]	Exp.[b]	Assignments[c]
ν_1	A′	1801.0 (0.4)	1797.6 (−3.0)	1804.6 (4.0)	1815.6 (15.0)	1816.0 (15.4)	1814.1 (13.5)	1801.0 (0.4)	1800.6	C=C stretch
ν_2	A′	1293.8 (−40.6)	1300.9 (−33.5)	1320.8 (−13.6)	1358.4 (24.0)	1358.8 (24.4)	1357.6 (23.2)	1339.0 (4.6)	1334.4	CF_2 (A) stretch
ν_3	A′	1178.2 (−38.0)	1183.4 (−32.8)	1196.9 (−19.3)	1238.0 (21.8)	1238.2 (22.0)	1237.1 (20.9)	1220.0 (3.8)	1216.2	C–F stretch
ν_4	A′	1036.8 (−22.9)	1038.7 (−21.0)	1051.7 (−8.0)	1077.7 (18.0)	1080.9 (21.2)	1079.7 (20.0)	1051.0 (−8.7)	1059.7	CF_2 (S) stretch
ν_5	A′	683.2 (−8.2)	686.0 (−5.4)	690.4 (−1.0)	693.8 (2.4)	693.9 (2.5)	693.3 (1.9)	687.0 (−4.4)	691.4	C–Cl stretch
ν_{10}	A″	550.6 (11.9)	564.3 (25.6)	560.1 (21.4)	525.6 (−13.1)	531.0 (−7.7)	530.3 (−8.4)	532.0 (−6.7)	538.7	(oop) CF_2 wag
ν_6	A′	510.1 (−6.1)	513.4 (−2.8)	516.2 (0.0)	516.7 (0.5)	516.6 (0.4)	516.3 (0.1)	515.0 (−1.2)	516.2	CF_2 bend
ν_7	A′	452.3 (−10.0)	453.5 (−8.8)	458.9 (−3.4)	464.9 (2.6)	464.9 (2.6)	464.7 (2.4)	459.0 (−3.3)	462.3	F(t)CCF(c) rock
ν_{11}	A″	369.6 (1.6)	376.3 (8.3)	378.2 (10.2)	366.8 (−1.2)	368.7 (0.7)	368.4 (0.4)	367.0 (−1.0)	368.0	(oop) CFCl wag
ν_8	A′	336.7 (−1.3)	337.8 (−0.2)	338.6 (0.6)	338.7 (0.7)	338.8 (0.8)	338.9 (0.9)	335.0 (−3.0)	338.0	CFCl bend
ν_9	A′	187.6 (−0.4)	188.5 (0.5)	189.6 (1.6)	186.0 (−2.0)	185.8 (−2.2)	186.9 (−1.1)	186.0 (−2.0)	188.0	CFCl rock
ν_{12}	A″	165.5 (−8.5)	167.6 (−6.4)	170.2 (−3.8)	165.6 (−8.4)	166.1 (−7.9)	166.3 (−7.7)	167.0 (−7.0)	174.0	(oop) torsion
MAE		12.5	12.4	7.2	9.1	9.0	8.4	3.8	0.0	

[a]In parenthesis, the signed errors are reported. Errors of harmonic frequencies computed with respect to the CCSD(T)/REF harmonic frequencies, errors of anharmonic frequencies evaluated with respect to experimental fundamentals. Mean Absolute Errors (MAE) derived by averaging over the absolute errors of each mode. In the case of modes affected by Fermi resonances, differences smaller than 10 cm^{-1} have been found between GVPT2 and deperturbed values.
[b]Tasinato *et al.*[20]
[c](A) and (S) refer to, respectively, Asymmetric and Symmetric modes, (oop) refers to out of plane bending modes, (c) and (t) stand, respectively, for cis- and trans-.
[d]Harmonic frequencies at the CCSD(T)/REF level, cubic and semi-diagonal quartic force constants at the B3LYP/SNSD level.
[e]Harmonic frequencies at the CCSD(T)/REF level, cubic and semi-diagonal quartic force constants at the B3LYP/cc-pVTZ level.
[f]Harmonic frequencies at the CCSD(T)/REF level, cubic and semi-diagonal quartic force constants at the B2PLYP/cc-pVTZ level.
[g]Geometry and second-order force constants at the CCSD(T)/ANOtz level, third- and fourth-order force constants at the CCSD(T)/cc-pVTZ level.

CCSD(T)/REF levels are collected, and the errors of the DFT results evaluated with respect to CCSD(T)/REF are also reported. The overall tendency of the DFT methods is to overestimate the harmonic integrated cross sections, and this trend is observed in the entire frequency range. In particular, in the HCBr bending zone (ν_4: 670–750 cm^{-1}) the intensities at the B3LYP/SNSD and B2PLYP/cc-pVTZ-PP levels are 125.49 and 120.40 km/mol, respectively, while a value of 103.00 km/mol is found at the CCSD(T) level. A similar trend is also observed in the 1050–1190 and 530–610 cm^{-1} frequency ranges. In the lower part of Table VIII, the anharmonic integrated cross sections are reported, as calculated at the DFT level and with both hybrid approaches. It is evident that only fully anharmonic computations allow to compare theoretical and experimental data in the spectral ranges where overtones and combination bands appear. By comparing our results with the experimental data,[18] a total MAE of about 6 km/mol for both DFT methods is observed, and the use of the hybrid approaches leads to MAEs of about 2 km/mol for both HYB^{B3D} and HYB^{B2T} intensities.

From the knowledge of the integrated cross sections together with the computed anharmonic frequencies, it is possible to simulate the entire IR spectrum by convoluting the intensity of each transition with either a Gaussian or Lorentzian function (see Sec. II A). For a quantitative comparison with the experimental spectrum, this procedure has been employed for $CHBrF_2$. The corresponding cross section spectrum in cm^2/molecule calculated at the B3LYP/SNSD level and using the hybrid approaches is plotted in Figure 8. Two regions of the spectrum have actually been considered, one between 600 and 1500 cm^{-1}, in which the transitions associated to the CF_2 stretching modes occur, and the other between 2000 and 3200 cm^{-1}, where in addition to the CH stretching modes also overtones and combination bands of the CF_2 stretching modes are evident. When the hybrid approach is applied to frequencies (compare DFT/DFT vs HYB/DFT spectra), a remarkable

TABLE X. Integrated cross sections (km/mol) of CF_2CFCl.

Harmonic integrated cross sections				
Range (cm^{-1})	Main transitions	B3LYP/ SNSD	B2PLYP/ cc-pVTZ	CCSD(T)/ REF
430–490	ν_7	0.42	0.44	0.94
490–575	ν_{10},ν_6	2.81	3.05	3.28
660–775	ν_5,$2\nu_{11}$	3.90	3.67	2.79
830–945	$\nu_{10}+\nu_{11}$	…	…	…
950–1120	ν_4,$2\nu_{10}$	241.19	233.70	222.97
1120–1168	$\nu_7+\nu_5$	…	…	…
1168–1275	ν_3,$\nu_9+\nu_4$	215.15	207.14	196.51
1280–1365	ν_2	185.74	172.61	160.12
1365–1450	$\nu_8+\nu_4$,$2\nu_5$	…	…	…
1450–1690	$\nu_7+\nu_4$	…	…	…
1690–1859	ν_1,$\nu_2+\nu_6$	60.92	61.36	56.04
1859–2220	$\nu_5+\nu_3$	…	…	…
2220–2510	$2\nu_3$,$\nu_4+\nu_2$	…	…	…
2510–2770	$2\nu_2$	…	…	…
2790–2885	$\nu_1+\nu_4$	…	…	…
2900–3065	$\nu_1+\nu_3$	…	…	…
MAE[a]		9.92	5.83	0.00

Anharmonic integrated cross sections						
Range (cm^{-1})	Main transitions	B3LYP/ SNSD	B2PLYP/ cc-pVTZ	HYB^{B3D}[b]	HYB^{B2T}[c]	Exp.[d]
430–490	ν_7	0.38	0.41	0.91	0.91	0.95
490–575	ν_{10},ν_6	2.74	3.01	3.21	3.24	3.16
660–775	ν_5,$2\nu_{11}$	4.25	4.09	3.14	3.20	3.30
830–945	$\nu_{10}+\nu_{11}$	1.56	1.45	1.56	1.45	2.82
950–1120	ν_4,$2\nu_{10}$	238.72	230.03	220.49	219.23	210.2
1120–1168	$\nu_7+\nu_5$	6.18	5.68	6.18	5.68	6.10
1168–1275	ν_3,$\nu_9+\nu_4$	208.60	199.98	189.96	189.35	189.0
1280–1365	ν_2	176.10	163.22	150.48	150.73	153.8
1365–1450	$\nu_8+\nu_4$,$2\nu_5$	2.55	3.00	2.55	3.00	3.83
1450–1690	$\nu_7+\nu_4$	4.41	3.61	4.41	3.61	4.7
1690–1859	ν_1,$\nu_2+\nu_6$	55.69[e]	57.49	50.81	52.17	55.2
1859–2220	$\nu_5+\nu_3$	4.97	4.03	4.97	4.03	4.06
2220–2510	$2\nu_3$,$\nu_4+\nu_2$	4.34	3.96	4.34	3.96	4.1
2510–2770	$2\nu_2$	2.78	0.36	2.78	0.36	2.86[f]
2790–2885	$\nu_1+\nu_4$	1.24	1.25	1.24	1.25	1.20
2900–3065	$\nu_1+\nu_3$	1.25	1.24	1.25	1.24	1.08
MAE[g]		4.82	3.16	1.47	1.39	0.00

[a]MAE of harmonic calculations evaluated with respect to the CCSD(T)/REF data.
[b]Harmonic intensities of fundamental modes empirically corrected at the CCSD(T)/REF level, B3LYP/SNSD intensities for all other modes.
[c]Harmonic intensities of fundamental modes empirically corrected at the CCSD(T)/REF level, B2PLYP/cc-pVTZ intensities for all other modes.
[d]Tasinato *et al.*[20]
[e]Resonance between modes $\nu_6+\nu_2$ and ν_1 manually removed.
[f]Experimental intensities in the 2510–2610 cm^{-1} (0.47 km/mol) frequency range have been summed to the experimental intensities in the 2610–2770 cm^{-1} (2.39 km/mol) frequency range in order to facilitate the assignment of the transitions.
[g]MAE of anharmonic calculations evaluated with respect to the experimental data.

improvement of the peak positions is observed. This is particularly evident in the CF_2 stretching modes (peaks B, C, E), with the peak E being entirely due to overtones and combination bands. On the other side, the hybrid approach applied to intensities yields only marginal corrections, as illustrated in Table VI. Finally, it is worth noting that the only empirical parameter used in Figure 8 for the visualization of the spectra is the FWHM of the Gaussian functions employed for the convolution of the peaks, which in this case has been arbitrarily fixed to 20 cm^{-1}.

In Table IX, the harmonic and anharmonic frequencies for the fundamental bands of CF_2CFCl are shown, as calculated at the B3LYP/SNSD, B3LYP/cc-pVTZ, and B2PLYP/cc-pVTZ levels, and compared with CCSD(T)/REF and experimental data. We note a small basis set effect in the DFT calculations, the MAE associated to the B3LYP/SNSD and B3LYP/cc-pVTZ methods being very similar at both the harmonic and anharmonic levels (about 12 cm^{-1} in all cases). By comparing B3LYP and B2PLYP calculations, very small differences are observed, the MAEs of the harmonic and

anharmonic frequencies at the B2PLYP/cc-pVTZ level being about 7 cm^{-1}. When the hybrid approach is applied, the MAEs of the frequencies become about 9 cm^{-1} in all cases. This value is slightly larger than the overall accuracy of the hybrid approach for frequencies (about 4 cm^{-1}, see Table V), and it can be related to the presence of many fluorine atoms as well as to inaccuracies in harmonic frequency calculations when a π charge distribution is involved (see Figure 1).

In Table X, the integrated cross sections are shown, as calculated at the B3LYP/SNSD and B2PLYP/cc-pVTZ levels as well as with hybrid approaches. In this case, the average errors are in line with the results reported in Table VI, the latter being about 4 km/mol at the DFT level and about 1 km/mol when the empirical hybrid correction is applied.

In Figure 9, the full IR spectrum in terms of cross sections is reported, as calculated at the B2PLYP/cc-pVTZ level and with hybrid approaches, and compared with experimental data. Analogously to the previous test case, a very good agreement on both peak positions and transition intensities is evident for all the computational level employed.

IV. CONCLUSIONS

In this work, we computed the infrared spectra of eight halogenated organic compounds, using the CCSD(T) level of theory as well as methods rooted in DFT, and compared the results with the available experimental data. In general, the spectra calculated at the DFT level show a good agreement with the experiments. In particular, at the B2PLYP/cc-pVTZ (-PP) level both frequencies and intensities are in remarkable agreement with both CCSD(T) and experimental results, while for B3LYP/SNSD in some cases peak positions show larger deviations. Correction of the harmonic terms by means of more accurate methods (such as CCSD(T) or B2PLYP/cc-pVTZ(-PP)) significantly improves the agreement. On the other side, intensities at the B3LYP/SNSD level are already in good agreement with experiments. A general conclusion that can be drawn from the present investigation is that DFT methods including both mechanical and electrical anharmonicity can be successfully used for the treatment of large systems also when halogen atoms are present, thus providing results in good agreement with experiment. Finally, it is further confirmed that the general approach of computing vibrational spectra beyond the double-harmonic approximation paves the route to routine simulation of realistic IR spectra for a wide set of molecular systems, including the species of atmospheric interest.

ACKNOWLEDGMENTS

The research leading to these results has received funding from the European Union's (EU) Seventh Framework Programme (FP72007-2013) under Grant Agreement No. ERC-2012-AdG-320951-DREAMS. This work has been supported by MIUR through the PRIN 2009 funding scheme: "Molecular Spectroscopy for Atmospherical and Astrochemical Research: Experiment, Theory and Applications." In detail, I.C. and C.C. acknowledge support from the Italian MIUR through the PRIN and FIRB founding scheme (PRIN 2009 – local project: Sviluppo di modelli accurati e di codici veloci per il calcolo di spettri vibrazionali – and FIRB-Futuro in Ricerca: Protocollo RBFR10Y5VW). In Venice, N.T., P.S., and A.P.C. gratefully acknowledge the financial support by PRIN 2009 (local project: Spettroscopia infrarossa a media e ad alta risoluzione di molecole di importanza atmosferica e astrofisica). In Bologna, C.P. acknowledges the financial supports by MIUR through the PRIN founding scheme (local project: Spettroscopia rotazionale di sistemi di interesse atmosferico e astrofisico: interplay tra esperimento e teoria) and by University of Bologna (RFO funds). The high performance computer facilities of the DREAMS center (http://dreamshpc.sns.it) are acknowledged for providing computer resources. The support of COST-CMST Action CM1002 "COnvergent Distributed Environment for Computational Spectroscopy (CODECS)" is also acknowledged.

[1] B. Sen, G. Toon, J.-F. Blavier, E. Fleming, and C. Jackman, J. Geophys. Res. **101**, 9045, doi:10.1029/96JD00227 (1996).
[2] A. Jain, B. Briegleb, K. Minschwaner, and D. Wuebbles, J. Geophys. Res. **105**, 20773, doi:10.1029/2000JD900241 (2000).
[3] D. McNaughton, E. Robertson, D. Thompson, T. Chimdi, M. Bane, and D. Appadoo, J. Anal. Chem. **82**, 7958 (2010).
[4] N. Christidis, M. Hurley, S. Pinnock, K. Shine, and T. Wallington, J. Geophys. Res. **102**, 19597, doi:10.1029/97JD01137 (1997).
[5] V. Naik, A. Jain, K. Pattern, and D. Wuebbles, J. Geophys. Res. **105**, 6903, doi:10.1029/1999JD901128 (2000).
[6] K. Sihra, M. Hurley, K. Shine, and T. Wallington, J. Geophys. Res. **106**, 20493, doi:10.1029/2000JD900716 (2001).
[7] E. A. Drage, D. Jaksch, K. M. Smith, R. A. McPheat, E. Vasekova, and N. J. Mason, J. Quant. Spectrosc. Radiat. Transf. **98**, 44 (2006).
[8] H. Zhang, J. Wu, and P. Lu, J. Quant. Spectrosc. Radiat. Transf. **112**, 220 (2011).
[9] S. Pinnock, M. Hurley, K. Shine, T. Wallington, and T. Smyth, J. Geophys. Res. **100**, 23227, doi:10.1029/95JD02323 (1995).
[10] E. Highwood and K. Shine, J. Quant. Spectrosc. Radiat. Transf. **66**, 169 (2000).
[11] K. Smith, D. Newnham, M. Page, J. Ballard, and G. Duxbury, J. Quant. Spectrosc. Radiat. Transf. **56**, 73 (1996).
[12] K. Smith, D. Newnham, M. Page, J. Ballard, and G. Duxbury, J. Quant. Spectrosc. Radiat. Transf. **59**, 437 (1998).
[13] G. Di Lonardo and G. Masciarelli, J. Quant. Spectrosc. Radiat. Transf. **66**, 129 (2000).
[14] J. Ballard, R. J. Knight, D. Newnham, J. V. Auwera, M. Herman, G. Di Lonardo, G. Masciarelli, F. Nicolaisen, J. Beukes, L. Christensen, R. McPheat, G. Duxbury, R. Freckleton, and K. Shine, J. Quant. Spectrosc. Radiat. Transf. **66**, 109 (2000).
[15] V. L. Orkin, A. G. Gushin, I. K. Larin, R. E. Huie, and M. J. Kurylo, J. Photochem. Photobiol., A **157**, 211 (2003).
[16] A. Pietropolli Charmet, N. Tasinato, P. Stoppa, A. Baldacci, and S. Giorgianni, Mol. Phys. **106**, 1171 (2008).
[17] P. Stoppa, A. Pietropolli Charmet, N. Tasinato, S. Giorgianni, and A. Gambi, J. Phys. Chem. A **113**, 1497 (2009).
[18] A. Pietropolli Charmet, P. Stoppa, N. Tasinato, A. Baldan, S. Giorgianni, and A. Gambi, J. Chem. Phys. **133**, 044310 (2010).
[19] N. Tasinato, P. Stoppa, A. Pietropolli Charmet, S. Giorgianni, G. Buffa, and A. Gambi, ChemPhysChem **12**, 356 (2011).
[20] N. Tasinato, A. Pietropolli Charmet, P. Stoppa, S. Giorgianni, and A. Gambi, Chem. Phys. **397**, 55 (2012).
[21] N. Tasinato, G. Regini, P. Stoppa, A. Pietropolli Charmet, and A. Gambi, J. Chem. Phys. **136**, 214302 (2012).
[22] S. Sekušak, K. Liedl, and A. Sabljić, J. Phys. Chem. A **102**, 1583 (1998).
[23] I. Ljubić and A. Sabljić, J. Phys. Chem. A **106**, 4745 (2002).
[24] I. Ljubić and A. Sabljić, J. Phys. Chem. A **109**, 2381 (2005).
[25] M. Baasandorj, G. Knight, V. Papadimitriou, R. Talukdar, A. Ravishankara, and J. Burkholder, J. Phys. Chem. A **114**, 4619 (2010).
[26] *Computational Strategies for Spectroscopy: From Small Molecules to Nano Systems*, edited by V. Barone (John Wiley & Sons, Inc., Hoboken, NJ, 2011).

[27] V. Barone, R. Improta, and N. Rega, Acc. Chem. Res. **41**, 605 (2008).
[28] A. Pedone, M. Biczysko, and V. Barone, ChemPhysChem **11**, 1812 (2010).
[29] V. Barone, A. Baiardi, M. Biczysko, J. Bloino, C. Cappelli, and F. Lipparini, Phys. Chem. Chem. Phys. **14**, 12404 (2012).
[30] J. Martin, T. L. Lee, P. Taylor, and J. Franois, J. Chem. Phys. **103**, 2589 (1995).
[31] A. Boese and J. Martin, J. Phys. Chem. A **108**, 3085 (2004).
[32] M. Biczysko, P. Panek, and V. Barone, Chem. Phys. Lett. **475**, 105 (2009).
[33] V. Barone, J. Chem. Phys. **120**, 3059 (2004).
[34] V. Barone, J. Chem. Phys. **122**, 014108 (2005).
[35] M. Biczysko, J. Bloino, G. Brancato, I. Cacelli, C. Cappelli, A. Ferretti, A. Lami, S. Monti, A. Pedone, G. Prampolini, C. Puzzarini, F. Santoro, F. Trani, and G. Villani, Theor. Chem. Acc. **131**, 1201 (2012).
[36] K. Peterson, D. Feller, and D. Dixon, Theor. Chem. Acc. **131**, 1079 (2012).
[37] H. H. Nielsen, Rev. Mod. Phys. **23**, 90 (1951).
[38] I. M. Mills, *Molecular Spectroscopy: Modern Research* (Academic, New York, 1972).
[39] A. D. Isaacson, D. G. Truhlar, K. Scanlon, and J. Overend, J. Chem. Phys. **75**, 3017 (1981).
[40] R. D. Amos, N. C. Handy, W. H. Green, D. Jayatilaka, A. Willets, and P. Palmieri, J. Chem. Phys. **95**, 8323 (1991).
[41] J. Vázquez and J. F. Stanton, Mol. Phys. **104**, 377 (2006).
[42] J. Bloino, M. Biczysko, and V. Barone, J. Chem. Theory Comput. **8**, 1015 (2012).
[43] J. Bloino and V. Barone, J. Chem. Phys. **136**, 124108 (2012).
[44] M. Biczysko, J. Bloino, I. Carnimeo, P. Panek, and V. Barone, J. Mol. Struct. **1009**, 74 (2012).
[45] A. Baldacci, P. Stoppa, A. Baldan, S. Giorgianni, and A. Gambi, J. Phys. Chem. A **113**, 6083 (2009).
[46] A. Baldacci, P. Stoppa, A. Pietropolli Charmet, J. Scaranto, and A. Gambi, Spectrochim. Acta, Part A **60**, 1967 (2004).
[47] A. Baldacci, P. Stoppa, A. Baldan, and A. Gambi, J. Mol. Struct. **827**, 165 (2007).
[48] *Many-Body Methods in Chemistry and Physics: MBPT and Coupled-Cluster Theory*, edited by I. Shavitt and R. Bartlett (Cambridge University Press, Cambridge, 2009).
[49] P. Carbonniere and V. Barone, Chem. Phys. Lett. **399**, 226 (2004).
[50] M. Biczysko, P. Panek, G. Scalmani, J. Bloino, and V. Barone, J. Chem. Theory Comput. **6**, 2115 (2010).
[51] V. Barone, M. Biczysko, J. Bloino, M. Borkowska-Panek, I. Carnimeo, and P. Panek, Int. J. Quantum Chem. **112**, 2185 (2012).
[52] I. Carnimeo, M. Biczysko, J. Bloino, and V. Barone, Phys. Chem. Chem. Phys. **13**, 16713 (2011).
[53] C. Puzzarini and V. Barone, J. Chem. Phys. **129**, 084306 (2008).
[54] C. Puzzarini and V. Barone, Phys. Chem. Chem. Phys. **10**, 6991 (2008).
[55] P. Carbonniere, T. Lucca, C. Pouchan, N. Rega, and V. Barone, J. Comput. Chem. **26**, 384 (2005).
[56] D. Begue, P. Carbonniere, and C. Pouchan, J. Phys. Chem. A **109**, 4611 (2005).
[57] D. Begue, A. Benidar, and C. Pouchan, Chem. Phys. Lett. **430**, 215 (2006).
[58] C. Puzzarini, M. Biczysko, and V. Barone, J. Chem. Theory Comput. **6**, 828 (2010).
[59] C. Puzzarini, M. Biczysko, and V. Barone, J. Chem. Theory Comput. **7**, 3702 (2011).
[60] V. Barone, M. Biczysko, J. Bloino, and C. Puzzarini, Phys. Chem. Chem. Phys. **15**, 1358 (2013).
[61] N. Tasinato, A. Pietropolli Charmet, P. Stoppa, S. Giorgianni, and G. Buffa, J. Chem. Phys. **132**, 044315 (2010).
[62] V. Barone, J. Bloino, and M. Biczysko, "Vibrationally-resolved electronic spectra in Gaussian 09" (2009), available online at http://dreamslab.sns.it/sites/default/files/download/docs/vibronic_spectra_G09-A02.pdf.
[63] V. Barone, J. Bloino, C. A. Guido, and F. Lipparini, Chem. Phys. Lett. **496**, 157 (2010).
[64] M. J. Frisch, G. W. Trucks, H. B. Schlegel, G. E. Scuseria, M. A. Robb, J. R. Cheeseman, G. Scalmani, V. Barone, B. Mennucci, G. A. Petersson, H. Nakatsuji, M. Caricato, X. Li, H. P. Hratchian, A. F. Izmaylov, J. Bloino, G. Zheng, J. L. Sonnenberg, M. Hada, M. Ehara, K. Toyota, R. Fukuda, J. Hasegawa, M. Ishida, T. Nakajima, Y. Honda, O. Kitao, H. Nakai, T. Vreven, J. A. Montgomery, Jr., J. E. Peralta, F. Ogliaro, M. Bearpark, J. J. Heyd, E. Brothers, K. N. Kudin, V. N. Staroverov, R. Kobayashi, J. Normand, K. Raghavachari, A. Rendell, J. C. Burant, S. S. Iyengar, J. Tomasi, M. Cossi, N. Rega, J. M. Millam, M. Klene, J. E. Knox, J. B. Cross, V. Bakken, C. Adamo, J. Jaramillo, R. Gomperts, R. E. Stratmann, O. Yazyev, A. J. Austin, R. Cammi, C. Pomelli, J. W. Ochterski, R. L. Martin, K. Morokuma, V. G. Zakrzewski, G. A. Voth, P. Salvador, J. J. Dannenberg, S. Dapprich, A. D. Daniels, Ö. Farkas, J. B. Foresman, J. V. Ortiz, J. Cioslowski, and D. J. Fox, Gaussian G09, Revision D.01, Gaussian, Inc., Wallingford, CT, 2009.
[65] K. Raghavachari, G. Trucks, J. Pople, and M. Head-Gordon, Chem. Phys. Lett. **157**, 479 (1989).
[66] J. T. H. Dunning, J. Chem. Phys. **90**, 1007 (1989).
[67] A. Kendall, J. T. H. Dunning, and R. Harrison, J. Chem. Phys. **96**, 6796 (1992).
[68] D. Woon and J. T. H. Dunning, J. Chem. Phys. **103**, 4572 (1995).
[69] J. Gauss and J. F. Stanton, Chem. Phys. Lett. **276**, 70 (1997).
[70] J. F. Stanton, J. Gauss, M. E. Harding, and P. G. Szalay, CFOUR, a quantum chemical program package, 2011; with contributions from A. A. Auer, R. J. Bartlett, U. Benedikt, C. Berger, D. E. Bernholdt, Y. J. Bomble, O. Christiansen, M. Heckert, O. Heun, C. Huber, T.-C. Jagau, D. Jonsson, J. Juselius, K. Klein, W. J. Lauderdale, D. Matthews, T. Metzroth, L. A. Mueck, D. P. ONeill, D. R. Price, E. Prochnow, C. Puzzarini, K. Ruud, F. Schiffmann, W. Schwalbach, S. Stopkowicz, A. Tajti, J. Vazquez, F. Wang, J. D. Watts and the integral packages MOLECULE (J. Almloef and P. R. Taylor), PROPS (P. R. Taylor), ABACUS (T. Helgaker, H. J. Aa. Jensen, P. Jorgensen, and J. Olsen), and ECP routines by A. V. Mitin and C. van Wuellen. For the current version, see http://www.cfour.de (accessed September 13, 2012).
[71] V. Barone, M. Biczysko, J. Bloino, and C. Puzzarini, J. Chem. Theory Comput. **9**, 1533 (2013).
[72] V. Barone, M. Biczysko, J. Bloino, and C. Puzzarini, Phys. Chem. Chem. Phys. **15**, 10094–10111 (2013).
[73] D. Tew, W. Klopper, M. Heckert, and J. Gauss, J. Phys. Chem. A **111**, 11242 (2007).
[74] M. Cortez, N. Brinkmann, W. Polik, P. Taylor, Y. Bomble, and J. Stanton, J. Chem. Theory Comput. **3**, 1267 (2007).
[75] K. Peterson, B. Shepler, D. Figgen, and H. Stoll, J. Phys. Chem. A **110**, 13877 (2006).
[76] K. Peterson, D. Figgen, E. Goll, H. Stoll, and M. Dolg, J. Chem. Phys. **119**, 11113 (2003).
[77] A. D. Becke, J. Chem. Phys. **98**, 5648 (1993).
[78] Double and triple-ζ basis sets of sns and n07 families, are available for download, 2012, visit http://dreamslab.sns.it (accessed April 1, 2013).
[79] V. Barone, P. Cimino, and E. Stendardo, J. Chem. Theory Comput. **4**, 751 (2008).
[80] V. Barone and P. Cimino, Chem. Phys. Lett. **454**, 139 (2008).
[81] V. Barone and P. Cimino, J. Chem. Theory Comput. **5**, 192 (2009).
[82] A. Bergner, M. Dolg, W. Kuchle, H. Stoll, and H. Preuss, Mol. Phys. **80**, 1431 (1993).
[83] G. Igelmann, H. Stoll, and H. Preuss, Mol. Phys. **65**, 1321 (1988).
[84] S. Grimme, J. Chem. Phys. **124**, 034108 (2006).
[85] F. Neese, T. Schwabe, and S. Grimme, J. Chem. Phys. **126**, 124115 (2007).
[86] C. Møller and M. S. Plesset, Phys. Rev. **46**, 618 (1934).
[87] S. Stopkowicz and J. Gauss, J. Chem. Phys. **129**, 164119 (2008).
[88] A. C. Brown, C. E. Canosa-Mas, A. D. Parr, K. Rothwell, and R. P. Wayne, Nature (London) **347**, 541 (1990).
[89] R. Talukdar, A. Mellouki, T. Gierczak, J. Burkholder, S. McKeen, and A. Ravishankara, Science **252**, 693 (1991).
[90] V. Orkin and V. Khamaganov, J. Atmos. Chem. **16**, 157 (1993).
[91] H. P. M. Filho and P. H. Guadagnini, J. Mol. Struct. **464**, 171 (1999).
[92] See supplementary material at http://dx.doi.org/10.1063/1.4817401 for tables collecting: coupled-cluster harmonic intensities of CH_2F_2 and CH_2CHF; valence angles of all the molecules; harmonic and anharmonic frequencies of CH_2F_2, CF_3Br, CH_2DBr, CH_2CHF, cis-CHFCHBr, cis-CHFCHI; harmonic and anharmonic intensities of CH_2F_2, CF_3Br, CH_2CHF.